Spectrum Sensing of FBMC Signals in 5G and Cognitive Radios

Thesis submitted in partial fulfillment
of the requirements for the degree of

Master of Science
in
Electronics and Communications Engineering by Research

by

Keesara Upender Reddy
201532549
keesara.upender@research.iiit.ac.in

International Institute of Information Technology
Hyderabad - 500 032, India
July 2018

International Institute of Information Technology
Hyderabad, India

CERTIFICATE

It is certified that the work contained in this thesis, titled "Spectrum Sensing of FBMC Signals in 5G and Cognitive Radios" by Keesara Upender Reddy, has been carried out under my supervision and is not submitted elsewhere for a degree.

_____ _____

Date Advisor: Dr. Sachin Chaudhari

To

My Family and Friends

Acknowledgements

I would like to acknowledge everyone who helped me and motivated me to write this thesis. I express my sincere gratitude to my advisor Dr. Sachin Chaudhari for his supervision throughout this work. His expertise and support has always motivated me to work harder. His encouragement has always been a ray of light amid many darkest passages that I have come across during the course of this work.

I thank the faculty of signal processing and communications research center (SPCRC): Dr. Lalitha Vadlamani, Dr. Prasad Krishnan, Dr. Rama Murthy Garimella and Dr. Ubaidulla P. I would also like to thank the SPCRC administrative head, Sailaja N, for her help in granting the funds for attending various conferences and workshops.

I thank my colleagues of SPCRC for their technical and non-technical discussions. Especially, I thank Zakir for the technical discussions that we had together. I thank Adarsh, Akhil, Anish, Deepa, Jayant, Kali, Madhuri Latha, Prudhvi, Rakesh, Vijay and Vivek. I thank Hari and Shiva for their valuable support and motivation that helped me keep going in the research work. I thank my friends Jagannadh, Maneesh, Murthy garu, Nachiket, Prakash, Prateek and Rhishi for making my stay at IIIT-H joyful. I will never forget the daily walks and parties we had together. Further, I thank Nachiket and Rhishi again for motivating me to take part in many marathons and cycling events which eventually kept me fit both physically and mentally.

I thank my friends Goutham, Surya, Tulasi and my brother Umesh for their support. Last but not least, I express my sincere gratitude to my beloved parents for their constant support and encouragement right through the completion of this thesis.

Abstract

Orthogonal frequency division multiplexing (OFDM) has been a dominant technology in several wireless standards such as LTE-A, WiMAX and WLAN. However, OFDM might be a misfit for next generation wireless communication systems (5G) and cognitive radios. OFDM suffers from drawbacks such as out of band radiation (due to high side lobe power), tight synchronization and loss in spectral efficiency. As a result of these disadvantages, OFDM is not going to be a default contender for 5G. In the recent past, many researchers have proposed filter bank multicarrier (FBMC) as a replacement for OFDM in 5G and cognitive radios. FBMC uses well designed bank of filters that has less side lobe power resulting in minimal out-of-band radiation so that the requirement of tight synchronization is relaxed in FBMC. This has a great advantage in machine-to-machine (M2M) communication and IoT.

Spectrum is a very scarce resource but unfortunately it is underutilized. Cognitive radio (CR) is one of the solutions to exploit the underutilized spectrum. Spectrum sensing is a key enabler for efficient use of spectrum and interference management in 5G and CR setting. In the spectrum sensing literature, there are no detection schemes available for FBMC signal except conventional energy detector. Hence, there is a need for feature detection techniques to efficiently detect FBMC signal.

In this work, we propose a spectrum sensing technique to detect FBMC signal in the presence of noise. Autocorrelation analysis of FBMC signal is carried out at each stage of FBMC signal generation. It is found that FBMC samples are correlated at last but one stage of FBMC signal generation. However, the autocorrelation value is zero for non-zero lag values at the last stage of FBMC signal generation. A modification is proposed to the received FBMC signal to retrieve the lost autocorrelation property of FBMC signal. With this modification, autocorrelation value at the lag equal to the number of subcarriers is non-zero. This autocorrelation property is used to design a detector for FBMC signal. The distribution of the test statistic of the proposed detector is derived under noise-only scenario so that the threshold of the detector can be obtained.

The performance evaluation of the proposed autocorrelation detector is carried out for different non-idealities such as multipath channel, noise uncertainty and no frame-synchronization (time). Next, the proposed detector's performance is compared with that of energy detector. Finally, the proposed detector is combined with the energy detector to increase the robustness of overall detection.

Contents

List of Figures

List of Tables

Abbreviations

ACF	Autocorrelation function
AWGN	Additive white Gaussian noise
BS	Base station
CAF	Cyclic autocorrelation function
CP	Cyclic prefix
CR	Cognitive radio
DFT	Discrete Fourier transform
DSA	Dynamic spectrum access
ED	Energy detector
E2E	End to end
FBMC	Filter bank multicarrier
FCC	Federal communications commission
FDM	Frequency division multiplexing
FFT	Fast Fourier transform
ICI	Inter carrier interference
IFFT	Inverse FFT
IID	Independent and identically distributed
IoT	Internet of things
ISI	Inter symbol interference
LDPC	Low density parity check
LOS	Line of sight
LTE-A	Long term evolution-advanced
MF	Matched filter
MIMO	Multiple input multiple output
mm	Milli meter
ms	Milli second
M2M	Machine to machine
NFV	Network function virtualization
NOMA	Non orthogonal multiple access
NR	New radio

OFDM	Orthogonal frequency division multiplexing
OFDMA	Orthogonal frequency division multiple access
OQAM	Offset quadrature amplitude modulation
PHY	Physical
PPN	Poly phase network
PU	Primary user
QoE	Quality of experience
RF	Radio frequency
SCF	Spectral correlation function
SDN	Software defined networking
SMS	Short message service
SMT	Staggered modulated multi tone
SU	Secondary user
SS	Spectrum sensing
SNR	Signal-to-noise ratio
UE	User equipment
WiMax	Worldwide interoperability for microwave access
WLAN	Wireless local area network

List of symbols

$\hat{a}$	Estimate of scalar a
a^*	Conjugate of scalar a
$\|a\|$	Modulus of a
B	Number of blocks present in FBMC signal
b	Block index
$E\{.\}$	Expectation operator
f	Frequency
g	Channel coefficient
H_0	Null hypothesis
H_1	Alternate hypothesis
$H(f)$	Frequency response of FBMC prototype filter
$h(n)$	Impulse response of FBMC prototype filter
$I(f)$	Frequency response of FFT filter
$\Im\{.\}$	Imaginary part of a complex number
i	Subcarrier index
K	Overlapping factor
m	Symbol index
N	Number of subcarriers, IFFT or FFT length
N_f	Number of blocks in FBMC steady state signal
N_s	Number of samples used for detection
$\mathcal{N}$	Gaussian distribution
n	Discrete time index
P	Multipath channel order
P_D	Probability of detection
P_{FA}	Probability of false alarm
$Pr(.)$	Probability function
$Q_{\chi^2_N}$	Central Chi-square distribution with N degrees of freedom
R_x	Autocorrelation of x
$\Re\{.\}$	Real part of a complex number
$S_i[mN]$	Input data symbol corresponding to ith subcarrier of mth symbol applied to IFFT block

T	Symbol duration
T_A	Test statistics for autocorrelation detector
T_E	Test statistics of energy detector
t	Discrete time index used for denoting steady state frame FBMC samples
$u(t)$	Modified received signal
$Var\{.\}$	Variance operator
$v(t)$	Received signal in presence of noise
$w(t)$	Additive white Gaussian noise samples
$w'(t)$	Modified AWGN samples
x_{1b}	IFFT output corresponding to input of bth block of chain-1
x_{2b}	IFFT output corresponding to input of bth block of chain-2
$y[n]$	Transmitted FBMC signal
$z(t)$	Modified FBMC signal
ρ	Correlation coefficient
δ	Indicator function used for division operation
γ	Threshold
τ	Time lag parameter
ϵ	Timing offset

Chapter 1

Introduction

1.1 Motivation

Invention of cellular technology is, undoubtedly, one of the major inventions of 20th century. Cellular technology has attracted much attention from many research groups all over the world. The first generation (1G) cellular system was introduced in 1980s. Since then the cellular technology has evolved from 1G to latest 4G standards to meet the demands of the people. However, with a growing demand for seamless connectivity with high data rates, the current 4G systems may become insufficient. So, there is a need for successor to 4G technology that efficiently meets the demands posed by the customers. In the recent past, researchers from various research groups, both from industry and academia, have started addressing the demands to be posed in near future in the field of wireless communication technologies. Some of the demands that are to be met are high data rates (multi fold than what 4G is providing today), low latency, ability to support billions of connected devices [1]. 5G, the next generation cellular technology, is expected to address these challenges [2, 3]. New air interfaces are one of the enablers of 5G to meet the afore mentioned challenges.

Orthogonal frequency division multiplexing (OFDM) has been a very important technology in cellular systems since last decade. However, OFDM is not spectrally efficient to be a contender for 5G. Use of cyclic prefix (CP) makes OFDM less spectrally efficient. OFDM uses rectangular pulses for pulse shaping leading to high side lobe powers of sinc signals in frequency domain. This spill over leads to inter channel interference (ICI). The multiple access version of OFDM, OFDMA, requires synchronization of different users in the network uplink to prevent ICI. Additional pilot symbols are to be transmitted for synchronization purpose. Also, signal processing schemes are to be employed to minimize the effect of synchronization errors. This leads to implementation complexity at OFDMA receivers. Many connected devices are expected to be in existence with the advent of internet of things (IoT) technology. Need of tight synchronization in OFDM may not be suitable for IoT set up. Moreover, OFDM is not an idle candidate for cognitive radio (CR) scenario because of high spectral leakage [4]. As a result of these drawbacks, OFDM is not going to be a primary candidate for 5G physical (PHY) layer. Hence, researchers have proposed new candidate waveforms for 5G PHY layer. One of such waveforms is filter

bank multicarrier (FBMC). FBMC is considered to be one of the promising alternatives to OFDM for future wireless communication systems and cognitive radio networks [2, 5, 6, 7, 8].

Efficient use of licensed spectrum is a key to effectively accommodate billions of connected devices and give high data rates to the users. CR is a possible solution to effectively utilize the spectrum and for interference management. CR is used to monitor the presence or absence of primary user (PU) signal before actually allocating the unused spectrum to the secondary users (SU). Hence, spectrum sensing of the licensed bands is an important task in the context of CRs. As such, spectrum sensing is a very relevant problem in the context of CR for 5G.

In spectrum sensing literature, most of the detection schemes have been designed for OFDM signal [9] and there is a dearth of research on spectrum sensing of FBMC signal. Although blind detection techniques such as energy detection may be used to detect any waveform, they cannot distinguish between noise and interfering signal. In addition they have serious issues such as SNR walls [10]. In [11], a feature detector was proposed based on the induced repeating patterns in the transmitted FBMC signal. Thus there is a lack of feature detectors for FBMC signal in the spectrum sensing literature. With this motivation, a feature detector is proposed in this work which can distinguish between FBMC-plus-noise and noise-only scenarios. Also unlike [11], no attempt is being made to induce patterns in the basic FBMC transmission.

1.2 Contributions of the thesis

The major contributions of this thesis are given below:

- The signal structure of FBMC signal is investigated thoroughly. It is observed that the FBMC waveform has inherent autocorrelation property. Next, autocorrelation analysis of FBMC signal is performed at each stage of FBMC signal generation to observe the autocorrelation among FBMC samples.

- It is found that the autocorrelation property that is inherent in FBMC samples is lost at the last stage of FBMC signal generation. Hence, an appropriate modification is proposed to get the autocorrelation back.

- The non-zero autocorrelation value at a non-zero lag, which is obtained after the proposed modification, is used to design a feature based detector to detect FBMC signal in the presence of noise.

- A test statistic is proposed for autocorrelation based detector and its distribution under noise-only case is derived so that the threshold for Neyman-Pearson detector can be evaluated.

- The proposed detector's performance is well investigated with the help of probability of detection vs signal-to-noise ratio (SNR) and receiver operating characteristics (ROC) curves.

- The performance evaluation of the proposed autocorrelation detector is carried out for different non-idealities such as multipath channel, noise uncertainty and no frame-synchronization.
- The the proposed detector's performance is compared with the performance of energy detector. Finally, the proposed detector is combined with the energy detector to increase the robustness of the detector in terms of increased probability of detection values.

1.3 Organization of the thesis

The organization of the thesis is given below:

- *Chapter 2*: An overview of 5G technology is presented in this chapter followed by a discussion on 5G specifications. Next, the necessary enablers of 5G are elaborated. Later, the concept of cognitive radio and spectrum sensing techniques are explained.
- *Chapter 3*: This chapter presents an overview on history of FBMC signal and types of FBMC signals. Next, FBMC signal generation is explained in detail followed by a comparison between OFDM and FBMC waveforms.
- *Chapter 4*: In this chapter, we first present signal structure of FBMC waveform. Next, a detailed autocorrelation analysis of FBMC signal has been carried out. Autocorrelation expressions at each stage of FBMC signal generation are derived. The derived theoretical expressions are verified through extensive simulations.
- *Chapter 5*: This chapter begins with the motivation for feature detectors followed by a discussion on the design of the proposed detector. Next, the performance of the proposed detector under certain non-idealities such as multipath channel, noise uncertainty and no frame-synchronization is presented with the help of extensive simulation results.
- *Chapter 6*: Conclusions of this thesis are presented in this chapter. Additionally, future scope for this work is discussed.

Chapter 2

5G and Cognitive Radio

This chapter provides an overview of 5G technology and CR. First, applications, challenges and enablers of 5G are presented. Next, a quick overview of CR is presented along with its key enabler spectrum sensing.

2.1 5G

The desire for broadband with high data rates has been the reason for evolution of cellular systems. Each generation of cellular networks has a killer application to support [2]. For example, voice communication in first generation cellular networks, short message service (SMS) in 2G, success of wireless LAN (WLAN 802.11) standards made the roads open for Internet connectivity in 3G because of widespread usage of laptops. In 4G, architecture was designed to provide high data rates to smart mobile phones. So, what is the killer application that 5G is going to provide? In fact, 5G will bring many key applications together in to existence.

2.1.1 5G applications

Few of the major applications that 5G will revolutionize are:

1. **High speed wireless connectivity:** With an exponential increase in demand for data rates by the users, 5G is expected to provide data rates of order of gigabits per second (Gbps). Such high speeds are expected even in the large crowd gathering areas such as shopping malls, railway stations etc.

2. **Tactile Internet:** Tactile internet includes many real time applications that require low latencies of order 1 ms. The word tactile Internet is motivated by the sensitivity perception of human beings who can distinguish latencies of order 1 ms. The latencies in current long term evolution-advanced (LTE-A) standard is of order of 10 ms. In 5G, the latencies are expected to be around 1ms to drive applications like robotic surgeries, autonomous driving etc., where low latencies are critical [2].

3. **IoT:** IoT is certainly going to play a major role in 5G. Smart wearables and smart home appliances assure a connected world. IoT has many applications in the fields such as agriculture, health care, transportation and many more. Although the current networks (2G/3G) support IoT requirements, many of the applications of IoT demand low latency, less energy consumption and high reliability which are not supported by existing networks [3]. Also, it is expected that there will be nearly 100,000 M2M nodes in a cell coverage [2]. As such, the barrier that IoT faces is transition to IPV6. 5G is expected to overcome this barrier to support many devices [12]. The other barrier for IoT development is scalability since the number of connected devices are going to be 20 billions by 2020. The frame work design for 5G in the context of IoT is detailed in [13].

The other applications that 5G provides include augmented reality, vehicle-to-vehicle communication, robotic surgery, autonomous cars and many more. In order to make the applications that are envisaged by 5G in to reality, certain challenges are to be addressed. These challenges are: high data rate, high capacity, low end-to-end (E2E) latency, massive device connectivity, reduced cost of operations and improved quality of experience (QoE).

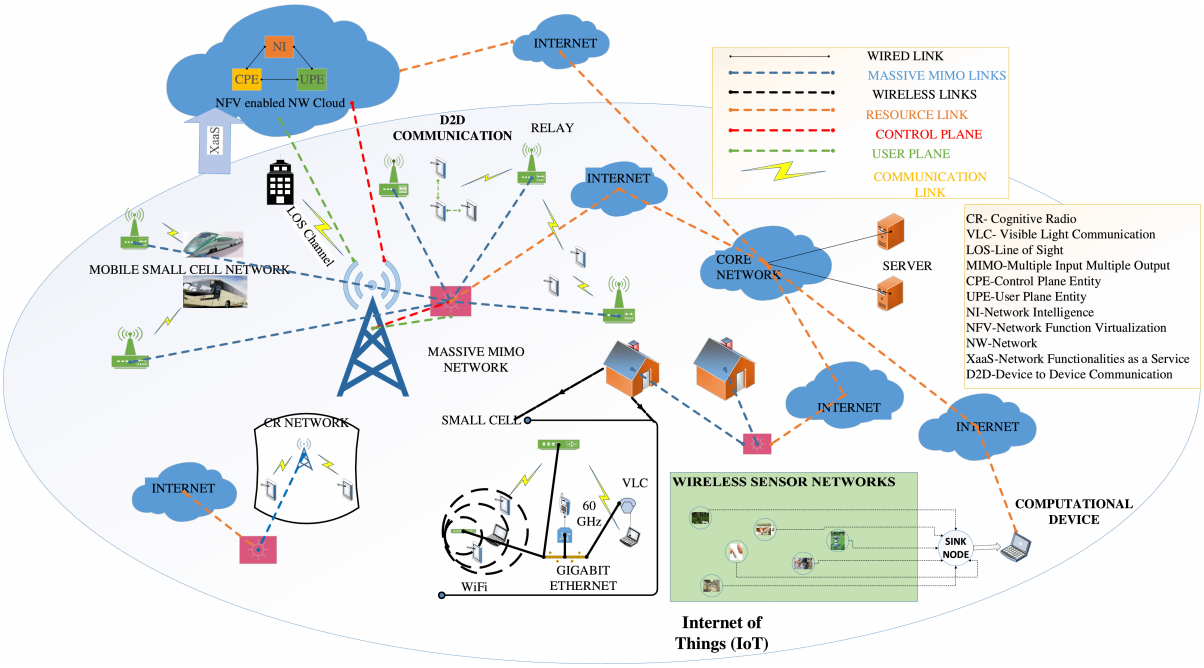

Figure 2.1: 5G network vision [1].

2.1.2 5G challenges

Few of the main challenges of 5G are:

System capacity and data rate

It is expected that by 2020 mobile networks need to assist the mobile traffic many times higher than current levels and provide 10-100 fold increased data rates even in high mobility conditions [14]. 5G is expected to provide data rates around 10 Gbps [15]. With increasing demands for high speeds, it is expected that there will be a problem of network congestion by 2020 [3]. Also, system capacity has to be improved to support many devices in a cell site.

E2E latency

In order to support the real time applications, E2E latencies are going to be critical. For example, remote controlled robots require quick feedback service to function well. Augmented reality and virtual reality applications require fast feedback and response time to get the real time sense. Also, the applications like vehicle to vehicle and vehicle to infrastructure communication require quick responses to ensure human safety. In order to support the afore mentioned use cases, the round trip latencies in 5G should be around 1 ms [16] where as the E2E latency in the current LTE-A systems is around 10 ms.

Massive number of connected devices

The advent of IoT has brought the provision of connecting many wearables and smart home appliances. As such, the number of these inter connected devices is likely to go up by 10-100 times beyond 2020 [17]. A few of these connected devices (sensors, for example) require sporadic connectivity for sending data to the devices that require always-on connectivity (e.g., cameras). The challenge here is to connect billions of diversified devices. In addition, the solutions have to be scalable and efficient.

Cost

Mobile phones and connectivity have become an integral part of human lives. So, it is important to decrease the infrastructure cost and the cost related to their deployment. The costs associated with deployment of infrastructure, maintenance and their operation are to be lowered to make connectivity a universal available and affordable service. In order to address the requirements posed by 5G, enormous improvements are needed which increases the cost of services that 5G offers. But, customers are not going to pay for the proportionate increase in the cost of maintenance. Hence, 5G network architecture is to be designed in such a way that it provides sustainable services to the customers with reduced cost.

One way to curtail the cost is to reduce the functionalities at the base stations. This can be achieved by performing only L1/L2 layer functionalities at the base stations and executing higher layers' operations at the common cloud that serves many base stations. This would reduce the cost of infrastructure deployment. Energy consumption is one of the cost drivers in a radio access network. Hence, energy efficient hardware designs and intelligent energy management techniques, such as making the base

stations to go to sleep mode when not in use, are to be developed to reduce the cost of operations in a 5G network.

QoE

QoE is another challenge that 5G must address. QoE describes the discernment of a user with regards to how good an application is working. QoE is entirely user and application specific. There is always an ambiguity in what is the QoE that user requires. Delivering an application with poor QoE leads to users' resentment. At the same time, having too high QoE may lead to draining of resources both at UE (battery power) and BS. Hence, a challenge in 5G would be to provide optimal QoE anytime and anywhere consistently.

2.1.3 5G enablers

In order to meet the 5G specifications, new technologies need to be adopted along with existing techniques. The following are the some of the important enablers of 5G.

New air interfaces and coding schemes

OFDM is currently the most popular technology for many of the existing wireless standards. However, use of CP makes OFDM less spectrally efficient. Also, with tight requirement for orthogonality and synchronization in OFDM, the coexistence of 5G and IoT may be in jeopardy. Hence, there is need for new waveforms that would successfully overcome the drawbacks of OFDM. FBMC is one such waveform that is considered to be an alternative to OFDM [7]. A detailed description of FBMC is presented in chapter 3.

By employing advanced modulation and coding schemes at physical layer, spectral efficiency and throughput can be improved. For example, spectral efficiency increases by choosing 256-quadrature amplitude modulation (QAM) with suitable coding techniques like low density parity check (LDPC) codes or polar codes [18, 19]. Such techniques can be combined together with massive multiple input multiple output (MIMO) to increase the system capacity. With extensive research being done to mitigate interference in macro cells, new multiple access schemes like non-orthogonal multiple access (NOMA) are expected to improve the system throughput by 30 percent compared to conventional orthogonal multiple access techniques [3, 20].

Massive MIMO

Massive MIMO is an upcoming technology which enlarges current MIMO systems by orders of magnitude [21]. With operating frequencies at the order of milli meter (mm) frequencies, more number of antennas can be exploited at BS. Such a sizeable number of antennas are arranged as arrays at the BS. Massive MIMO with two dimension (2D) antenna array can be exploited to increase the cell coverage by

employing three dimension (3D) beamforming techniques using steerable antennas [22, 23]. Massive MIMO system can increase the capacity of a network 10 times or even more [21]. However, there are many research problems associated with massive MIMO that are to be extensively studied to make massive MIMO technology a reality. The challenges are fast signal processing, pilot contamination, hardware impairments and channel modeling. Significant research must be carried out to come up with better solutions to these challenges.

mm-waves

The fast increase in the growth of mobile data is creating many challenges to the network providers. As the need for high quality and low latency videos is growing day by day, the spectrum available to support these applications is limited. The available spectrum for cellular communication ranges from 700 MHz to 2.6 GHz [24]. Many research studies propose that mm-wave frequency bands might be used to expand the currently occupied 700 MHz to 2.6 GHz radio frequency bands for wireless communications [25]. The band of frequencies from 3-300 GHz are referred as mm-wave bands as the wavelengths associated with these frequencies range from 1-100 mm. With the use of mm-waves, the bandwidth available will be increased manifolds to achieve higher data rates. The availability of unlicensed spectrum at 60 GHz has paved the way for providing Gbps data rates [25]. With these high frequency bands, more number of antennas can be exploited at the base station (BS) using massive MIMO technology to increase cell capacity [21]. The feasibility of mm-wave communication is possible by steerable antennas both at the BS and user equipments (UEs). However, high frequency bands are susceptible to path loss and absorption by objects. Also, the propagation is limited to line of sight (LOS) paths and short ranges. These shortcomings are to be addressed properly to make use of mm-waves in 5G.

Network densification is another solution to increase system capacity and data rates [3]. Deploying many small cells gives rise to network densification. As stated earlier, with the carrier frequencies being at mm range, the path losses and absorption losses are high. These disadvantages of mm-waves are considered advantageous in small cell scenarios. mm-waves with massive MIMO technique can be efficiently used to improve system throughput in small cells [14]. So, mm-wave communication is treated as an enabler to increase cell system throughput and data rates.

NFV and SDN

Network function virtualization (NFV) and software defined networking (SDN) are feasible enablers to reduce the cost of operations. NFV is claimed to reduce network complexity. NFV separates network functionalities from hardware and implements them on software with dedicated cloud servers [26]. Similarly, SDN provides network optimization. Both NFV and SDN make the network adaptable as any new upgrades can be implemented with necessary changes in the software [3]. The flexibilities offered

by these two technologies ease the network deployment and make the overall network flexible. Thus a network can be easily deployed and the cost of infrastructure can be reduced.

Cognitive radio

Spectrum is a scarce resource and unfortunately it is very much underutilized [27]. As the demand for data rates is growing further day-by-day, it is important to efficiently utilize the spectrum to meet the demands of the customers. As such, CR is seen as a solution for spectrum scarcity problem [27]. Spectrum sensing is an important task in CR to identify the unoccupied frequency bands [9]. A detailed description of CR and spectrum sensing is presented in Sections 2.2 and 2.3, respectively.

2.2 Cognitive radio overview

The traffic growth has increased multi fold in the recent past due to increased number of mobile devices. In order to meet the demands of users for high data rates, efficient use of spectrum is a key. However, the spectrum is utilized inefficiently. This inefficiency in spectrum usage arises mainly because of static spectrum allocations and fixed regulations. CR is proposed as a novel solution to improve the spectrum usage. CR is a technology which enables the users to efficiently utilize the spectrum by continuously monitoring the spectrum [27]. As per the definition of Federal communication commission (FCC), "Cognitive Radio: a radio or system that senses its operational electromagnetic environment and can dynamically and autonomously adjust its radio operating parameters to modify interference, facilitate interoperability, and access secondary markets [28]".

2.2.1 CR applications

The major applications of CR are: dynamic spectrum access and coexistence of heterogeneous networks (interference management).

Dynamic spectrum access

In CR terminology, the user who owns the spectrum is called primary user (PU) and the user who uses the unlicensed spectrum in the absence of PU is called the secondary user (SU). A SU can use the PU spectrum when the spectrum is vacant. A SU, using the spectrum of a PU, has to vacate the spectrum whenever the PU requires it. One of the challenges in CR is to reduce the interference so that the performance of the PU is not deteriorated. The SUs opportunistically use the spectrum of different PUs to meet the bandwidth requirements. Such an opportunistic use of spectrum is called 'dynamic spectrum access (DSA)'. DSA is very much important to solve the problem of spectrum scarcity [29]. Three important components of DSA are: Spectrum awareness, spectrum access and cognitive processing.

- **Spectrum awareness**: Spectrum awareness is responsible for opportunistically selecting the unoccupied frequency bands that are dynamic in time, frequency and space [30, 31]. The main task in spectrum awareness is to find if a particular band of frequency is free or not. If it is occupied, it is important to know the parameters of the transmitter such as location, power etc. The awareness about the spectrum can be obtained by utilizing geolocation databases or by spectrum sensing locally at CR.

- **Spectrum access**: In Spectrum access, the SUs utilize the available spectrum based on the spectrum awareness performed. As many CR users try to access the unoccupied spectrum, it is important to have spectrum management techniques for spectrum access to limit the interference among the CR users. The spectrum management process has four important steps to successfully mitigate the interference: spectrum sensing, spectrum decision, sharing of spectrum, spectrum mobility [32]. A detailed description of spectrum management is discussed in [32].

- **Cognitive processing**: Cognitive processing involves decision making by intelligently performing certain tasks like radio environment awareness, efficient spectrum sensing and handling interference for coexistence of SU and PU [32].

Interference management

Coexistence of many heterogeneous networks lead to interference in 5G environment. 5G is expected to have network tiers of different cell sizes, transmit power levels, back-haul connections [33]. Along with these enhanced techniques, massive MIMO technology will be adopted in 5G networks to increase the cell capacity in order to serve different users simultaneously [21]. However, such networks with massive MIMO technology are prone to co-tier interference and cross-tier interference which eventually degrades the performance of the intended users [22, 34]. The current state of the art interference cancellation techniques such as channel allocation, power control and load balancing may not be effective to mitigate the interference in heterogeneous and multi-tier 5G networks [33]. Thus, there is a need to develop efficient interference management techniques for 5G networks as the employed standards, waveforms and transmission powers are different for different networks [35].

CR is a novel solution for interference management in 5G networks [27, 36]. Cognitive capabilities allow a user to identify the presence or absence of other users by performing spectrum sensing such that the interference caused to the other existing users is minimal. Effective resource allocation and management techniques for CR are proposed in [37]. In [38, 39], an attempt is being made to mitigate the interference in heterogeneous networks by enabling dynamic frequency selection and optimal power allocation using CR. Thus, CR is seen as an effective solution for interference management in 5G.

2.3 Spectrum sensing

DSA is one of the key applications of CR. Spectrum sensing (SS) is a principal enabler in cognitive radios for DSA. SS helps prevent interference of SU with PU. SS should identify the spectrum holes (unoccupied frequency bands) to enhance the throughput and quality of service. Hence, the detection performance is important in SS aspect for better performance of CR. As such, the detection performance is quantified by two parameters: probability of false alarm (P_{FA}) and probability of detection (P_D). P_{FA} is defined as probability that a CR declares PU is present where spectrum is actually free [40]. P_D is defined as probability that a CR declares PU is present when the spectrum is occupied by PU [40]. These two metrics are very crucial for a CR setting. A miss in the detection causes interference to the PU while false alarm minimizes the spectral efficiency.

As stated earlier, SS techniques should identify the spectrum holes to improve spectral efficiency. There are two types of spectrum holes: temporal spectrum holes and spatial spectrum holes. A temporal hole arises if a PU frequency band is unused (i.e., no transmission by PU) for a period of time. During this period SUs can exploit the unused frequency band. Spatial hole arises if a PU's transmission is limited to a particular range and hence SU can use the same frequency band for parallel transmission, in time, outside the coverage area of PU to nullify the interference with the PU.

2.3.1 Spectrum sensing classification

In order to know the presence of PU, SS is to be performed to know the spectrum occupancy information. Different spectrum sensing approaches are mentioned in [41, 42, 43, 44] for obtaining spectrum occupancy information. The SS techniques depend on primary transmitter detection. A classification of SS schemes is shown in Fig. 2.2. Transmitter detection is performed locally at a CR and the CR decides the presence of PU by observing the PU transmitted signal. On the other hand, in cooperative detection, multiple CRs cooperate to take a decision about spectrum occupancy. Each CR contributing to the detection performs SS locally and shares the sensing data in the CR network. Based on the way of sharing sensing data, the cooperative detection is classified in to three types: centralized, distributed and relay assisted [45]. Depending on the application, a CR may choose for wide band sensing or narrow band sensing. Thus, the main focus of SS will be on determining narrow band spectrum hole or wide band spectrum hole. Proactive sensing refers to periodic sensing of spectrum by a CR and the reactive sensing refers to spectrum sensing by a CR when ever there is a demand for sensing. Apriori information availability is an important criterion for classification of SS techniques. Based on the availability of apriori information of transmitted PU signal, SS can be classified as non-blind, semi-blind and total-blind. Non-blind SS schemes need PU signal structure and noise power estimate to detect PU. Semi-blind techniques need only noise power estimates to spot a spectrum hole. Total-blind SS schemes require no information about the PU signal and noise variance. Fig. 2.3 illustrates different SS techniques grouped based on apriori information and wide band/narrow band sensing.

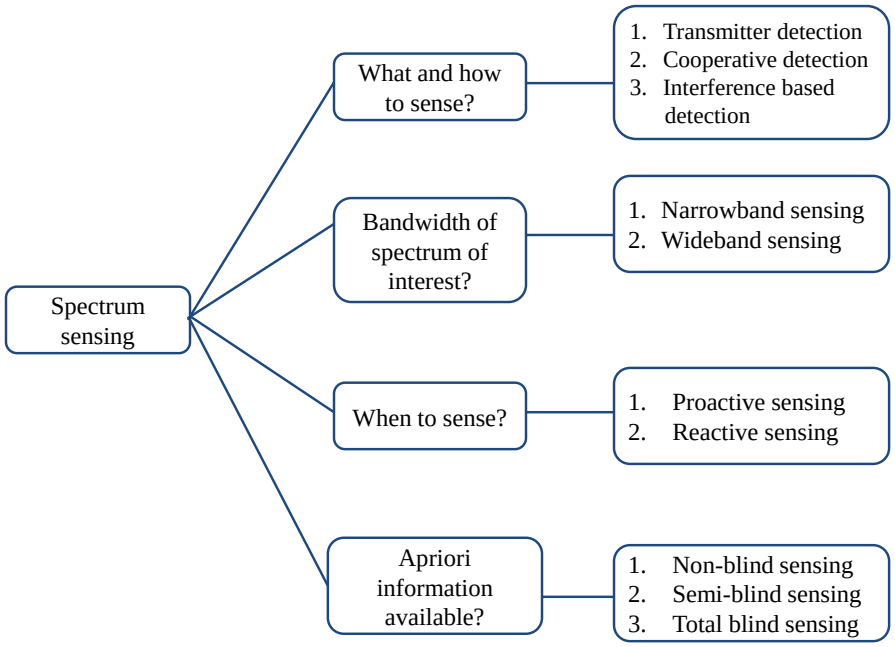

Figure 2.2: Classification of spectrum sensing schemes [41].

Generally, detection problem is modeled as binary hypothesis testing model given as:

$$\begin{aligned} H_0: &\quad y[n] = w[n] \\ H_1: &\quad y[n] = x[n] + w[n], \end{aligned} \tag{2.1}$$

where $y[n]$ is the received signal, $x[n]$ is the transmitted signal and $w[n]$ is additive white Gaussian noise (AWGN) with 0 mean and σ_w^2 variance. H_0 is called null hypothesis and H_1 is called alternate hypothesis. H_0 represents that PU is absent while H_1 represents that spectrum is occupied with in the frequency band that is being scanned by CR. In general, a spectrum can be occupied by a PU or other SU. Hence, it is important not only to detect the PU but also to differentiate between PU and SU. Performance of the detector depends on type of SS technique chosen. Three main detection techniques employed for SS are: energy detection, feature detection and matched filter detection.

Energy detection

Energy detector (ED) is suitable for wide band SS [41]. The basic approach in ED is that the signal at the receiver is initially applied to a bandpass filter to select the frequency band for sensing. Energy of the filtered signal is calculated and compared with a threshold (γ) to know the presence of PU. A detailed description of ED is presented in [46]. If T represents the test statistics for the ED, the detector chooses H_1 if $T > \gamma$ or chooses H_0 if $T < \gamma$. The test statistics T for ED is given as

$$T = \frac{1}{N_s} \sum_{n=0}^{N_s-1} |y[n]|^2, \tag{2.2}$$

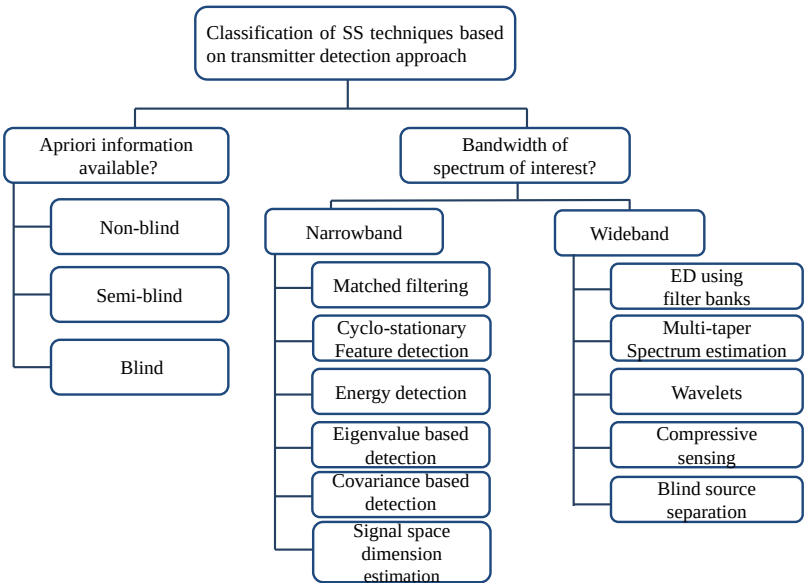

Figure 2.3: Spectrum sensing techniques [41].

where N_s is number of samples considered for detection. Proper care is to be taken to choose the threshold γ. If γ is too low, the P_{FA} $(Pr(T > \gamma|H_0))$ increases which refers to underutilization of spectrum holes. If γ is high then the P_D $(Pr(T > \gamma|H_1))$ is low resulting in interference with PU. Hence, there is a trade off in considering the threshold [40]. Practically, P_{FA} is fixed to a low value $(< 10^{-1})$ and P_D is maximized.

PU's information is not essential in ED. Hence, it is a blind detector. ED needs only the estimate of noise variance to set a threshold value for the detection. However, the major limitation of ED is noise uncertainty that results in uncertainty in threshold. In practical scenarios, the knowledge of noise power is unknown and the detector will only have an estimate of noise power. This imperfect knowledge of noise variance is known as "noise uncertainty". The limitations like noise uncertainty [47] and SNR walls (i.e., minimum SNR below which signals can not be detected) [10] in ED paves way for better detection methods which makes use of one or more features of PU.

Feature detection

Feature detection based SS technique relies on capturing a particular pattern of PU (Cyclic prefix in OFDM for example) for spectrum sensing. The basic feature based detectors are cyclostationary detector and autocorrelation detector. Many of the practical wireless signals are combined with sine wave carriers, pulse trains, cyclic prefixes (in OFDM signals) which introduce periodicities in the signals which make the signals cyclostationary. This periodicity generally arises from inducing repeating patterns to estimate channel (pilot symbols) or symbols which are used for synchronization. The cyclostationary feature detection makes use of periodicity property of received signals to detect PU in the presence of noise.

The inbuilt periodicity of cyclostationary signals makes statistical properties like mean and autocorrelation repeat with a pattern. The cyclostationary property introduces correlation among received samples of PU which can be observed using cyclic autocorrelation function (CAF) or can be equivalently viewed in frequency domain as spectral correlation function (SCF) [48]. Many cyclostationary based algorithms use peaks induced by CP for detection of PU signals. For standard waveforms like OFDM, the length and location of CP is known. However, SUs may employ OFDM signals with almost equal symbol duration and CP length. Hence, cyclostationarity information is not reliable to differentiate between PU and SU. Authors in [49] have proposed a robust algorithm to differentiate PU and multiple SUs which use OFDM modulation. Second-order cyclostationarity property is exploited in [49] to classify PU and SU.

The other prominent feature detector is autocorrelation based detector. Similar to cyclostationary detector, autocorrelation detector also uses the inherent correlation existing among the samples of the communication signals. The difference between cyclostationary and autocorrelation detectors is that the former uses the particular repeating patterns (cyclostationarity) of the signal where as the latter uses the stationary correlation values of a signal [50, 51, 9]. The autocorrelation based detectors are less complex to implement compared to cyclosationary detectors [9].

The notable feature of cyclostationary detector and autocorrelation detector is that they can differentiate PU from interference (SU) and noise. They can also distinguish different PU signals. Another advantage of feature detectors is that they are very much robust to noise uncertainty. In low SNR regime, feature detector outperforms ED [41]. However, the accuracy of feature detectors comes with increased implementation complexity. High sensing time is also a drawback in feature detectors.

Matched filter detection

Matched filter (MF) detection is a type of coherent sensing method. Coherent sensing exploits known patterns of PU to coherently detect PU. These known patterns may be pilot symbols which are deliberately introduced in PU signals to estimate channel properties and to minimize synchronization errors (time and frequency) at the receiver. If a CR has the apriori information of these patterns of PU signal then the PU can be detected by passing the received signal to a filter having the impulse response matched to the received signal. This technique is known as "matched filter technique". The coherent detection can also be carried out by correlating the signal at the receiver with itself to extract the induced patterns. It is proved in [52] that coherent processing of received samples would detect very weak signals. However, in order to perform MF detection, the cost of having pilot symbols to maintain synchronization is to be incurred.

2.3.2 Choosing a SS method

The choice of selecting a SS method has a trade off between accuracy and complexity. When the apriori knowledge of PU signal is not available then ED is the best and simple detector. However,

ED is not robust to fading scenarios and noise uncertainties. Some information about PU is required to distinguish PU from SU and noise. Exploiting this information about PU makes detection reliable with increased computational cost. Such techniques are called non-blind techniques and the choice of choosing a non-blind method depends on available information about PU. For example, cyclostationary method is suitable if the cyclic frequencies of PU are known while coherent detection is preferable if information about pilot transmissions is known apriori.

Chapter 3

FBMC: A contender for 5G

In this chapter, we first present history and various types of FBMC signals. Next, an overview of multicarrier transmission is detailed followed by a detailed discussion on FBMC signal generation. Finally, a comparison between OFDM and FBMC is presented.

3.1 FBMC signal

3.1.1 History of FBMC signal

FBMC has been in existence since the early 20th century. There are many types of filter bank techniques implemented in the literature [53, 54]. Staggered-modulated multitone (SMT) type of filter bank is very popular for the reason that the spectral efficiency of SMT method is better compared to other methods. The pioneering work in SMT FBMC was carried-out by Chang [55] and Saltzberg [56] in 1960s. They showed that it is possible to get back the symbols at the receiver with out any ISI and ICI by transmitting in-phase and quadrature-phase components with a delay equal to half the symbol duration. Further work in FBMC was done by Hirosaki [57], who demonstrated the efficient implementation of offset QAM (OQAM)-filter bank method by poly phase network (PPN) structure of discrete Fourier transform (DFT). With this motivation for the SMT method, in this thesis, we considered the SMT implementation of FBMC signal. Interested readers are referred to [5, 58, 59, 60, 61] for more details on background and implementation of FBMC signal.

3.1.2 Multicarrier transmission

In a multicarrier transmission, OFDM for example, inverse fast Fourier transform (IFFT) and fast Fourier transform (FFT) algorithms are used as a transform pair to modulate and demodulate the data, respectively. As shown in Fig. 3.1, the input to IFFT block of length N is $S_i[mN]$ with $0 \leq i \leq N-1$.

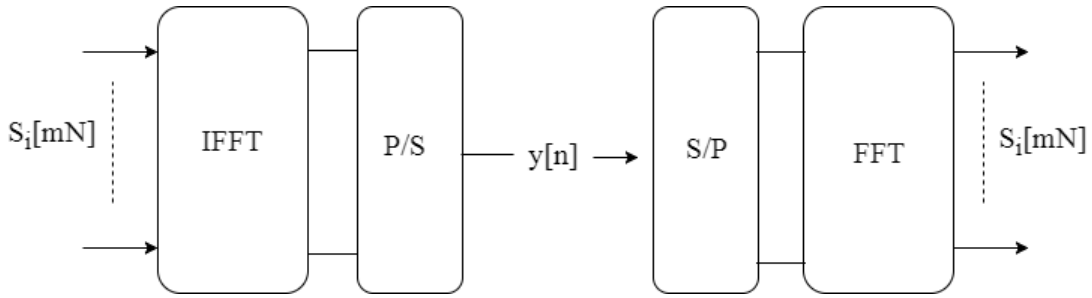

Figure 3.1: Multicarrier transmission.

For $mN \leq n \leq (m+1)N$, the output of IFFT is given by the expression

$$y[n] = \sum_{i=0}^{N-1} S_i[mN] e^{\frac{j2\pi ni}{N}}. \tag{3.1}$$

Here, m represents the symbol index [58]. A parallel-to-serial converter is used to transmit the IFFT samples serially in to the channel. At the receiver, a serial-to-parallel conversion is performed and parallel samples are applied to FFT block to obtain the input data samples. The input data samples are obtained by

$$S_i[mN] = \frac{1}{N} \sum_{n=mN}^{mN+N-1} y[n] e^{-\frac{j2\pi ni}{N}}. \tag{3.2}$$

The proper functioning of the system depends on the timing synchronization of both the transmitter and the receiver. However, in a practical scenario like multipath propagation the received samples are delayed by the respective delay timings. Hence, the received samples interfere either constructively or destructively. In this scenario, it is not possible to demodulate the received samples using FFT alone because the ISI has been introduced due to the multipath propagation and the orthogonality nature of the carriers is lost. So, how to overcome the problem of ISI? There are two solutions given in [62]:

1. Increase the symbol duration by inserting guard time to be more than channel impulse response's length and demodulate with the FFT. This approach is known as OFDM. In OFDM, CP is used as guard interval to eliminate ISI.

2. Keep the duration of the symbol same but do some processing to the FFT [58]. This approach is called FBMC.

3.1.3 FBMC signal generation

Rectangular pulse is applied as filter in a conventional OFDM system in time-domain [4]. One drawback of pulse shaping used in OFDM is its out-of-band radiation. The out-of-band ripples can be reduced by introducing more frequency coefficients such that the main lobe of filter-frequency-response at each subcarrier is spread while side lobes are reduced so that only adjacent subchannels overlap. As

overall frequency spread of the response reduces significantly because of frequency spreading operation, the impulse response of the filter in time-domain spreads beyond one symbol duration and the symbols overlap in time domain. The number of symbols which overlap in time domain is given by the parameter K, known as *overlapping factor*. Here, the challenge is to design a prototype filter [1] which successfully aids for ISI free transmission of data symbols in spite of overlapping of the symbols.

Prototype filter design

The fundamental principle behind the prototype filter design for ISI free transmission is the Nyquist criterion. Let $h(t)$ be the channel impulse response, then the condition for zero ISI is given from [63] as

$$h(nT) = \begin{cases} 1; & n = 0 \\ 0; & n \neq 0 \end{cases}, \tag{3.3}$$

where T is the symbol period. This is equivalent to

$$\frac{1}{T} \sum_{k=-\infty}^{+\infty} H(f - \frac{k}{T}) = 1 \quad \forall \quad f, \tag{3.4}$$

with $H(f)$ being the Fourier transform of $h(t)$. The intuition of Nyquist criterion is: "the frequency shifted versions of $H(f)$ should add up to a constant value". In practice, if the base band filters satisfy Nyquist criterion then the data elements can be transmitted over a channel that has a flat response, with zero ISI. From (3.3), Nyquist criterion can also be interpreted as "the impulse response of the filter must cross the zero axis at the integer multiples of the symbol period [58]". This condition, in frequency domain, is nothing but having the symmetry of the frequency response around the cutoff frequency, which is half the symbol rate. Now, the prototype filter is designed with the frequency coefficients that satisfy the Nyquist symmetry condition in frequency domain. The coefficients of prototype filter are obtained as [64]:

$$\begin{aligned} &H_0 = 1 \quad ; \quad H_l^2 + H_{K-l}^2 = 1 \quad ; \quad 1 \leq l \leq K-1 \\ &H_{KN-l} = H_l \quad ; \quad 1 \leq l \leq K-1 \\ &H_l = 0 \quad ; \quad K \leq l \leq KN-K, \end{aligned} \tag{3.5}$$

where N denotes number of subcarriers while K represents overlapping factor. Using (3.5) the frequency coefficients for $K = 2,\ 3,\ 4$ are given in table 3.1. In this work, the *overlapping factor* considered is 3. The frequency response $H(f)$ is given by [62]

$$H(f) = \sum_{k=-(K-1)}^{K-1} H_k \frac{\sin(\pi(f - \frac{k}{NK})NK)}{NK \sin(\pi(f - \frac{k}{NK}))}, \tag{3.6}$$

and is presented in Fig. 3.2(a) for $N = 64$ subcarriers. It is evident from the figure that the out-of-band

[1] first filter in the filter bank

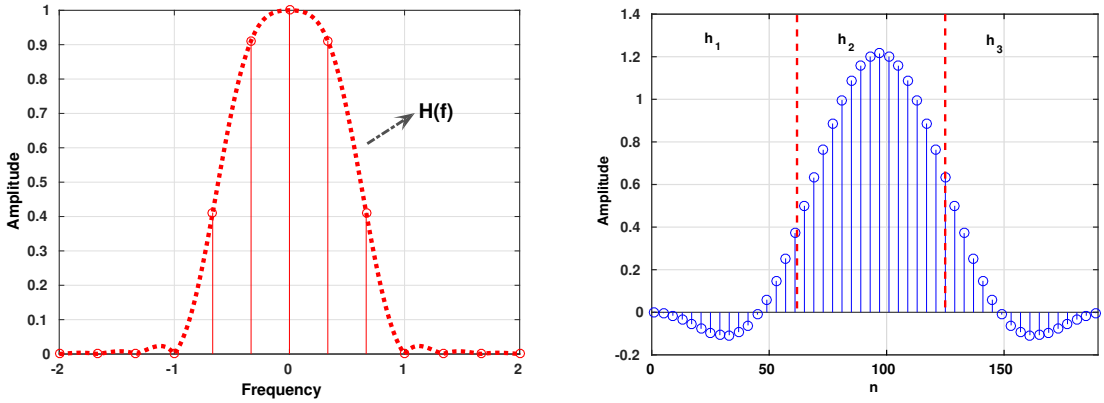

(a) Frequency response $H(f)$

(b) Impulse response $h[n]$

Figure 3.2: Prototype filter response in frequency domain and time domain for $K = 3$ and $N = 64$ [62].

ripples are insignificant. The corresponding impulse response $h[n]$ of length $KN = 192$ samples is obtained by frequency sampling technique [62] and is given by

$$h[n] = H_0 + 2\sum_{k=1}^{K-1} H_k \cos\left(\frac{2\pi kn}{KN}\right), \tag{3.7}$$

for $n = 0, 1, \ldots, KN-1$ and is shown in Fig. 3.2(b). The figure also exhibits three equal partitions of $\mathbf{h}$, viz., $\mathbf{h}_1$, $\mathbf{h}_2$, $\mathbf{h}_3$ that play a crucial role in simplifying the analysis in the later sections.

Now, the bank of filters is obtained by frequency shifting the prototype filter frequency response with $\frac{k}{N}$ as shown in Fig. 3.3. The k^{th} filter in the bank is obtained by multiplying the frequency coefficients of the prototype filter with $e^{\frac{j2\pi ki}{N}}$. A portion of the filter bank obtained is shown in Fig. 3.3. In the figure, the X-axis corresponds to subcarrier index (also referred as sub-channels in FBMC) with the subcarrier spacing as unity and the Y-axis corresponds to the magnitude of the filters. The even index (or odd index) sub-channels are not overlapping. Moreover, a sub-channel overlaps with its neighboring sub-channels only [58]. Hence, orthogonality is essential among adjacent sub-channels.

K	H_0	H_1	H_2	H_3
2	1	$\frac{\sqrt{2}}{2}$	-	-
3	1	0.911438	0.411438	-
4	1	0.971960	$\frac{\sqrt{2}}{2}$	0.235147

Table 3.1: Frequency domain prototype filter coefficients.

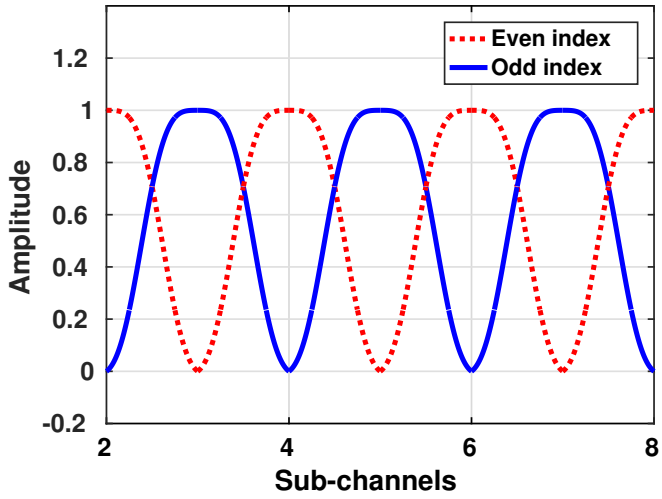

Figure 3.3: Portion of filter bank for $K = 3$.

OQAM modulation

In FBMC, any modulation technique can be used as long as the adjacent subcarriers are not overlapping. If even index (or odd index) subcarriers are used then the subcarriers do not overlap. However, to seek full capacity of the system all the subcarriers are to be utilized. A modulation technique is required to nullify the effect of overlapping of adjacent subcarriers by maintaining orthogonality among adjacent subcarriers. Orthogonality among the adjacent subcarriers is preserved by using the real part of the complex input symbols with even index subcarriers of IFFT and the imaginary part of the complex input symbols with odd index subcarriers [58]. Here, the system capacity is reduced by a factor of 2 as only real or imaginary part of a complex symbol is transmitted at any time instant. Full capacity of the system is achieved in the following way: double the symbol rate and each subcarrier is loaded with the real and imaginary part of a complex symbol. Here, the real and imaginary components are transmitted at different time instants with a time delay equal to half the symbol period. It is noteworthy that data can be transmitted using the real part of the subcarrier i at unit spacing rate and using the imaginary part of the subcarrier i at unit spacing rate but with a shift of half the symbol duration. Similarly, data transmission is done on subcarriers $i-1$ and $i+1$ but with the interchange of real and imaginary parts of the input complex symbols. This scheme is known as OQAM technique. Fig. 3.4 illustrates the implementation of OQAM technique. The term "offset" implies to the delay introduced in the transmission of real and imaginary components of a complex symbol.

In OFDM, each data element given to the subcarrier of $N-$size IFFT block modulates a single carrier, whereas in FBMC each data element applied to $KN-$size IFFT modulates $2K-1$ subcarriers due to the overlapping factor K. Thus, single data component is spread over many IFFT inputs. This operation is known as *weighted frequency spreading* [62]. As shown in Fig. 3.5, input element $S_i[mN]$ modulates $2K-1$ carriers centered at the iK^{th} subcarrier. For each set of N input samples IFFT

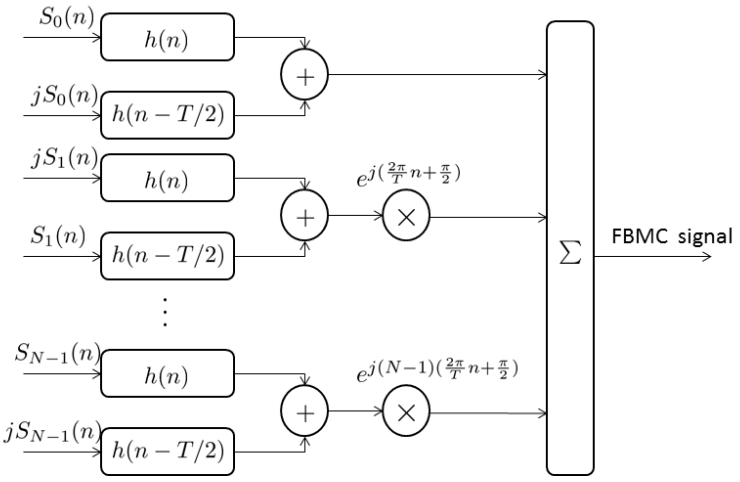

Figure 3.4: OQAM technique. Here, T is symbol period. In this thesis, $T = N$.

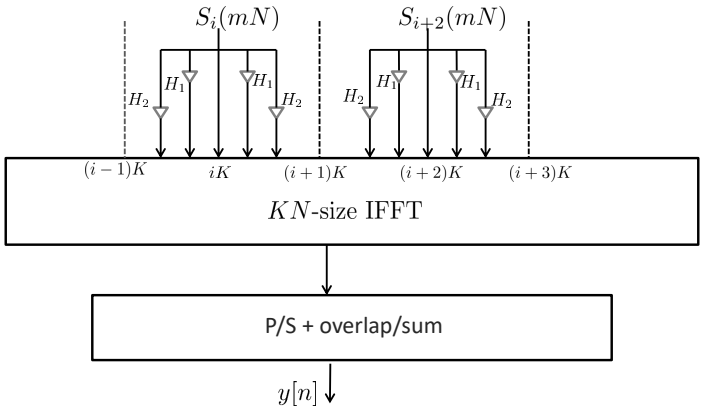

Figure 3.5: Simple block diagram of FBMC transmitter with weighted frequency spreading and extended IFFT for $K = 3$ [62]. Loading of $(i+1)K^{th}$ subcarrier is not shown for convenience.

produces KN samples. Since the symbol rate is $\frac{1}{T} = \frac{1}{N}$, K symbols overlap in the time domain. Hence, the output of filter bank is supplied with the overlap and sum operation as shown in Fig. 3.5. From Fig. 3.5, it is evident that the subcarriers i and $i+2$ do not overlap where as the subcarrier $i+1$ overlaps with both i and $i+2$. So, orthogonality is required among adjacent subcarriers. Orthogonality is provided by OQAM technique as explained earlier.

At the receiver, the data recovery is determined based on Nyquist filter's property:

$$\frac{1}{N}\sum_{k=-(K-1)}^{K-1}|H_k|^2 = 1. \tag{3.8}$$

The receiver block diagram of FBMC is the reverse of transmitter section with IFFT block being replaced by FFT block. The issue with this transmitter-receiver structure is its complexity because of

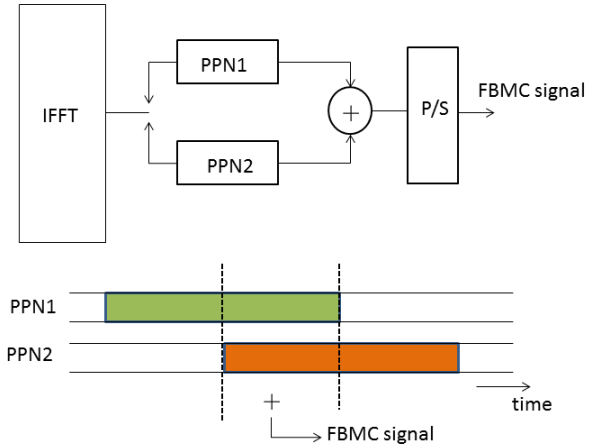

Figure 3.6: PPN-FFT approach [62].

extended IFFT and FFT blocks from N to KN. An efficient way of reducing the computational complexity is to use PPN-FFT approach. In this method, the FFT length is kept as N and additional processing called PPN (poly phase network) is introduced. The PPN-FFT approach is implemented in [62]. As explained in [62], PPN-FFT approach needs two chains or a single IFFT functioning at twofold increased rate integrated with two PPN sections as shown in Fig. 3.6. The output symbols, each of N samples, coming out of PPN1 chain and PPN2 chain overlap by $N/2$ samples. Hence, an adder is put in place.

3.2 OFDM Vs FBMC

The magnitude response of OFDM and FBMC prototype filter is shown in Fig. 3.7(a) [4, 58]. From Fig. 3.7(a), it is clear that the magnitude of side lobe of FBMC prototype filter for $K = 4$ is very much less than that of OFDM. The side lobe power of FBMC for $K = 4$ is 20 dB less than that of OFDM. Hence, $K = 4$ exhibits better spectral resolution. However, the side lobe magnitude of FBMC filter for $K = 2$ is very much comparable to that of OFDM. Hence, $K = 2$ may not be suitable for cognitive radio scenarios in which spectral resolution of waveform of PU is expected to be good. Fig. 3.7(b) depicts the complexity comparison of OFDM and FBMC system for various K values. The trade off for choosing K values is implementation complexity and the side lobe power of the prototype filter. The complexity of FBMC system is high compared to that of OFDM system. This is the cost that has to be paid while moving from OFDM to FBMC waveform. In FBMC system, $K = 4$ has high complexity

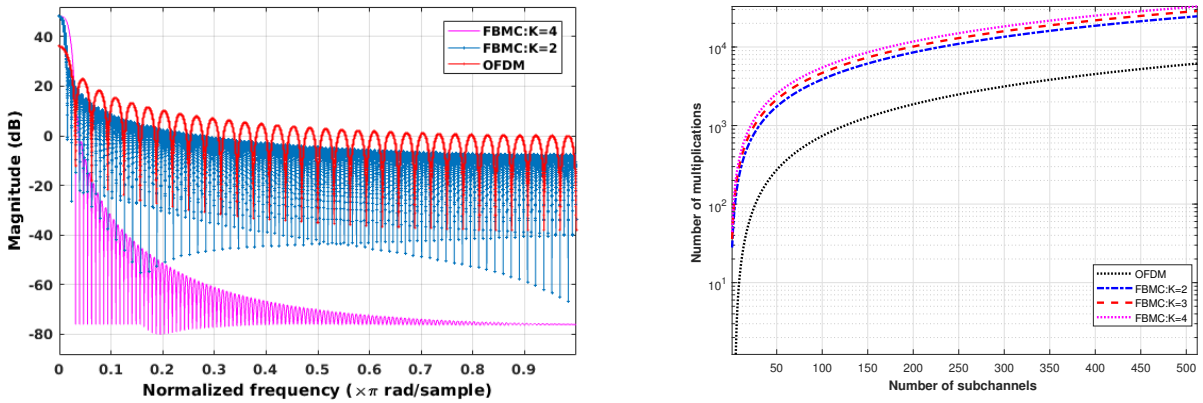

(a) Magnitude response

(b) Complexity comparison

Figure 3.7: Magnitude response and complexity comparison of prototype filters of OFDM and FBMC.

while $K = 2$ has low complexity. Complexity of $K = 3$ is in between complexity of $K = 4$ and $K = 2$.

The multiple access version of OFDM (OFDMA) works fine in down link. However, because of power leakage into adjacent SC each user is to be synchronized at the BS to avoid ICI. Additional signal processing is to be performed in a network uplink scenario to maintain synchronization. This signaling overhead is an issue in an IoT setup [13]. Also, because of high side lobe power, it is difficult for a CR to distinguish between PU and SUs. Hence, FBMC with better spectral resolution is proposed to suit applications of 5G and CR [6, 58].

Chapter 4

Autocorrelation Analysis of FBMC signal

In this chapter, we first present the FBMC signal structure followed by the autocorrelation analysis of FBMC signal at the transmitter. It is shown that autocorrelation values at last stage of FBMC signal generation are zero for non-zero lags. Later, a modification is proposed to the received FBMC signal to get back the non-zero autocorrelation at a lag equal to the number of subcarriers. Finally, we present autocorrelation analysis of modified FBMC signal with $K = 2$.

4.1 FBMC signal structure

In this section, we explain the FBMC signal generation described and implemented in [65], which is helpful in finding the structure in the FBMC signal, which in turn can be detected using a feature detector. Note that the implementation of weighted frequency spreading shown in Fig. 3.5 can be achieved by first loading every K^{th} subcarrier with data and then convolving with frequency response $H(f)$ of prototype filter. In time domain, this is equivalent to repeating the time-domain data block K times and then multiplying the resultant data vector of length KN with $\mathbf{h}$. This approach is used in this thesis to obtain the FBMC signal and is shown in Fig. 4.1.

As shown in Fig. 4.1, there are two chains for generating FBMC signal (Note that these two chains will be replaced by two PPNs in low-complexity FBMC implementation as explained in [62]). Complex input symbols, $S_b[i]$ corresponding to block or symbol b, are fed to N-IFFT block of both chain-1 and chain-2 sections. In chain-1, real part of $S_b[i]$ is loaded on i^{th} subcarrier if i is odd while imaginary part (including j) of $S_b[i]$ is loaded on the i^{th} subcarrier if i is even. On the other hand, for chain-2, imaginary part (including (j) of $S_b[i]$ is loaded on i^{th} subcarrier if i is odd while real part of $S_b[i]$ is loaded on the i^{th} subcarrier if i is even. The chain-1 data vector corresponding to b^{th} block is represented by $\mathbf{x}_{1b}$. Each output block of KN samples of chain-1 and chain-2 overlap by $\frac{N}{2}$ samples and the samples are added to give the transmitted FBMC signal $y[n]$. Here, $y[n] = y_1[n] + y_2[n - N/2]$ where $y_1[n]$ and $y_2[n]$ are the outputs of chain-1 and chain-2, respectively.

Fig. 4.2 shows a representative example of the frame structure of FBMC signal assuming $K = 3$ and input data blocks $\mathbf{S}_b$ of N samples with block index $b = 1, 2, \ldots, 7$. Each block is delayed by

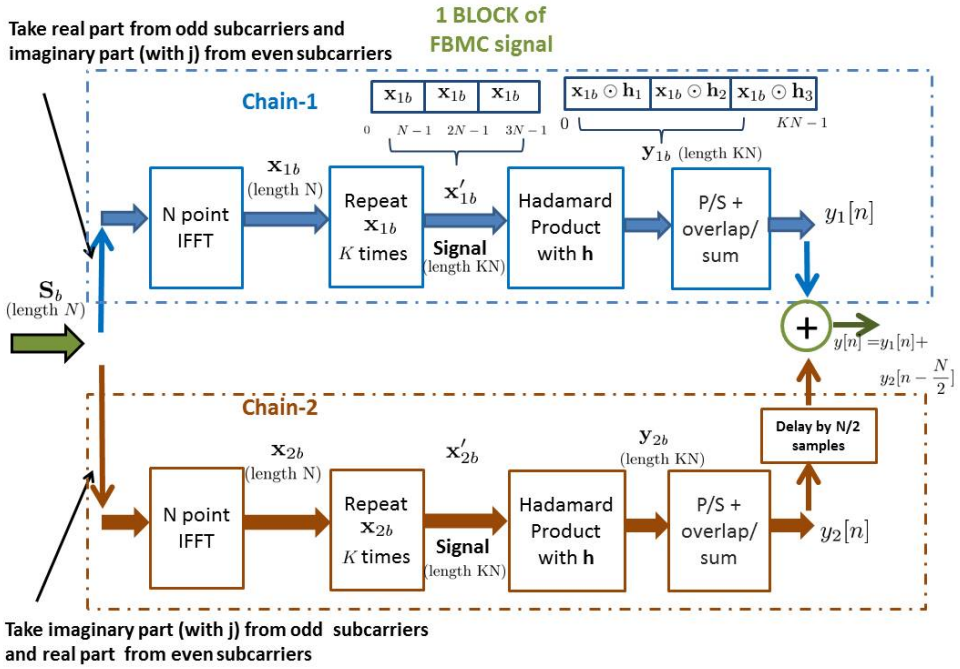

Figure 4.1: FBMC signal generation: This figure shows the generation of b^{th} block of data samples for $K = 3$. Each input block ($\mathbf{s}_b$) is of length N samples and output block ($\mathbf{y}_{1b}$ or $\mathbf{y}_{2b}$) is of length KN samples. Output samples of chain-2 are delayed by $N/2$ samples and are added to output samples of chain-1 to give corresponding b^{th} block output.

N samples to its preceding block and blocks are overlapped to give final output for chain-1 frame. Generation of FBMC signal for chain-1 frame is shown in Fig. 4.2. Generation of chain-2 signal is similar and only the resulting chain-2 frame is shown for conciseness. Finally, the signals from chain-1 and chain-2 (delayed by $N/2$ samples) are added to give the final transmitted FBMC signal. Note that the autocorrelation analysis has to be performed on a *steady state frame*, which is defined as part of the transmitted frame containing K number of overlapped symbols for both chain-1 and chain-2 outputs. A steady state frame is obtained by removing KN samples, from the overlapped frames, at the beginning and $(K-1)N$ samples at the end. This steady state frame is considered for autocorrelation calculations in the following sections.

4.2 Autocorrelation analysis of transmitted FBMC signal

In this section, autocorrelation of FBMC signal is analyzed at each stage of the signal generation as described in Fig. 4.1. As this chapter focuses only on analyzing the autocorrelation function (ACF) for FBMC signal, we assume noise-free channel in this chapter so that the transmitted as well as received FBMC signals are the same. Also, the autocorrelation properties are derived only for the output of four stages (IFFT, repetition, Hadamard Product and P/S + overlap/sum) of chain-1. Due to similarity in

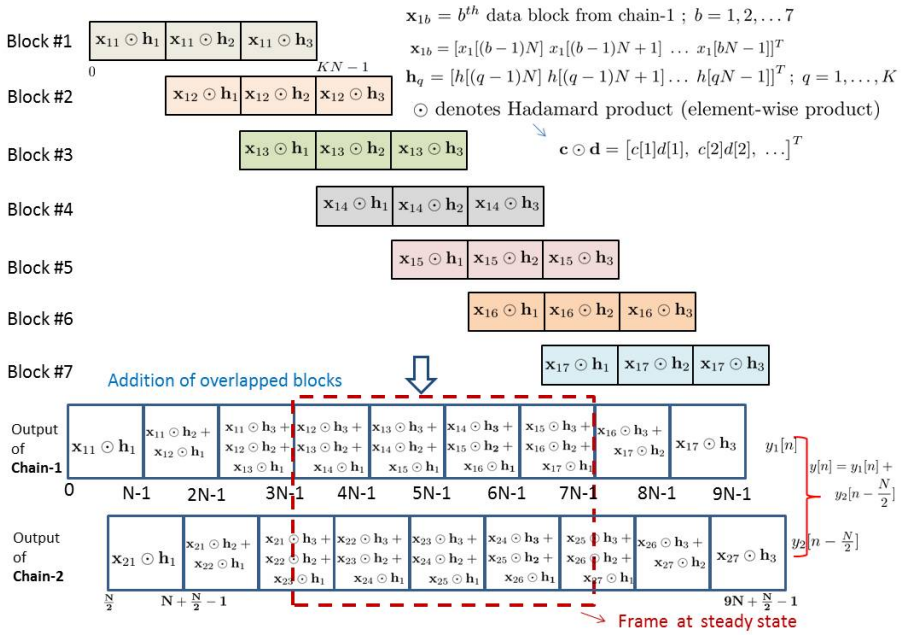

Figure 4.2: FBMC frame structure: In this figure, generation of chain-1 signal is shown using data-blocks. Generation of chain-2 signal will be similar and only the resulting chain-2 frame is shown. Here, $K = 3$, number of blocks = 7.

the operations of the two chains, the autocorrelation properties of the output of corresponding stages of chain-2 will be same. The autocorrelation of the sum of the two chains will be derived at the end.

4.2.1 Autocorrelation of $\mathbf{x}_{1b}$

We assume that complex symbols $S_b[i]$ (such as QAM) for $i = 0, \ldots, N-1$, each with variance σ_s^2, are fed to $N-$point IFFT. In chain-1, real part of $S_b[i]$ is loaded on the i^{th} subcarrier if i is odd while imaginary part (including j) of $S_b[i]$ is loaded on the i^{th} subcarrier if i is even. Therefore, input to $N-$point IFFT are the random variables $\mathcal{R}(S_b[i])$ or $j\mathcal{I}(S_b[i])$ with variance $\sigma_s^2/2$ based on subcarrier index i being even or odd. For sufficiently large N, the output of IFFT $x_{1b}[n]$ can be approximated as independent and identically distributed (IID) Gaussian random variables as shown in [51] such that

$$x_{1b}[n] \sim \mathcal{N}_c(0, \sigma_{x1}^2), \tag{4.1}$$

where $\sigma_{x1}^2 = \sigma_s^2/2$ and $\mathcal{N}_c$ denotes distribution for complex circular symmetric Gaussian random variable. The autocorrelation function of $x_{1b}[n]$ is given by

$$R_{x_{1b}}(n, \tau) = E\{x_{1b}[n]\, x_{1b}^*[n+\tau]\} = \begin{cases} \sigma_{x_1}^2 = \sigma_s^2/2 & \tau = 0 \\ 0 & \tau \neq 0 \end{cases}, \tag{4.2}$$

where n, τ and b are all integers with $n \in [0, 1, \ldots, N-1]$ and $b \in [1, \ldots, B]$ while $0 \leq n+\tau < N-1$. Here B is the number of data blocks.

4.2.2 Autocorrelation of $\mathbf{x}'_{1b}$

It is evident from Fig. 4.1, that $\mathbf{x}'_{1b}$ is generated by repeating $\mathbf{x}_{1b}$ K times. As such, the autocorrelation function of $x'_{1b}[n]$ is given by

$$R_{x'_{1b}}(n,\tau) = E\{x'_{1b}[n]\, x'^{*}_{1b}[n+\tau]\} = \begin{cases} \sigma_{x_1}^2 = \sigma_s^2/2 & \tau = \pm kN \\ & \text{s.t. } 0 \leq n+\tau < KN \\ 0 & \text{Otherwise} \end{cases}, \tag{4.3}$$

for $n \in [0, KN-1]$ while $k \in [0, 1, \ldots, (K-1)]$. Here, *s.t.* refers to *such that*. Fig. 4.3(a) shows the simulated autocorrelation values for $\mathbf{x'}_{1b}$ with $K = 3$ and $N = 64$. The simulated autocorrelation values match very well with the theoretical autocorrelation values in (4.3). Moreover, it can be clearly seen that the samples of $\mathbf{x}'_{1b}$ are uncorrelated, except for $\tau = 0, \pm N, \pm 2N$ as theory suggests.

4.2.3 Autocorrelation of $\mathbf{y}_{1b}$

As shown in Fig. 4.1, the next step is element-wise multiplication (Hadamard product denoted by $\odot$) of $\mathbf{x'}_{1b}$ with the frequency-spreading-filter impulse response $\mathbf{h}$, both of size KN, i.e., $\mathbf{y}_{1b} = \mathbf{x'}_{1b} \odot \mathbf{h}$. The autocorrelation of $\mathbf{y}_{1b}$ is given by

$$\begin{aligned} R_{y_{1b}}(n,\tau) &= E\{y_{1b}[n]\, y^{*}_{1b}[n+\tau]\} \\ &= E\{x_{1b}[n]\, h[n]\, x^{*}_{1b}[n+\tau]\, h^{*}[n+\tau]\} \\ &= E\{x_{1b}[n]\, x^{*}_{1b}[n+\tau]\}\, h[n]\, h[n+\tau] \\ &= \begin{cases} \frac{\sigma_s^2}{2}\, h[n]\, h[n+\tau] & \tau = \pm kN \\ & \text{s.t. } 0 \leq n+\tau < KN \\ 0 & \text{Otherwise} \end{cases}, \end{aligned} \tag{4.4}$$

for $n \in [0, KN-1]$ and $k \in [0, K-1]$. Here the last step is due to (4.3). Note that $h[n]$ is a real valued function so that $h^*[n] = h[n]$. Fig. 4.3(b) shows the autocorrelation plot of $\mathbf{y}_{1b}$ for various values of n and τ for $K = 3,\ N = 64$. The simulated values match well with theoretical values from (4.4). Observe that autocorrelation values are non-zero for $\tau = 0, \pm N, \pm 2N$ for $K = 3$ although the values at the lag $\pm 2N$ are negligible as compared to those at the lags of 0 and $\pm N$.

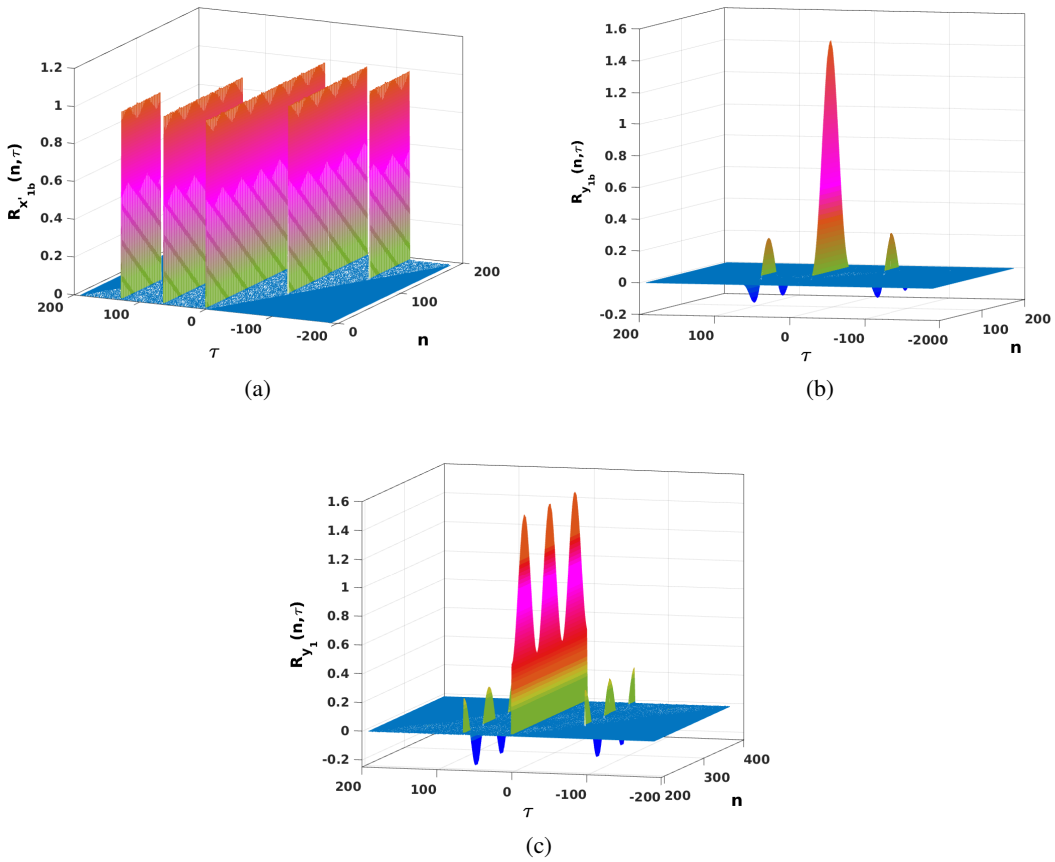

Figure 4.3: Simulated autocorrelation values at output of different stages of chain-1 for $N = 64$, $K = 3$, and the number of Monte-Carlo realizations = 100000: (a) The samples of $x'_{1b}[n]$ are correlated for time lags of $0, \pm N, \pm 2N$. (b) The samples of $y_{1b}[n]$ are correlated for time lags of $0, \pm N, \pm 2N$. However, correlation values at the lag $2N$ are negligible compared to that of N. (c) The samples of $y_1[n]$ are correlated for time lags of $0, \pm N$. Again, correlation at lags of $\pm 2N$ are negligible.

4.2.4 Autocorrelation of $y_1[n]$ after overlap and add of K data blocks

In overlap and add, data for K blocks are overlapped and added. For the steady state part of frame, after overlap and add operation (see Fig. 4.2), we have

$$\begin{aligned} y_1[n] &= y_1[(b-1)N + l] \\ &= \sum_{k=0}^{K-1} y_{1(b-k)}[l + kN] \\ &= \sum_{k=0}^{K-1} x_{1(b-k)}[l + kN]\, h[l + kN] \\ &= \sum_{k=0}^{K-1} x_1[(b-k)N + l]\, h[l + kN], \end{aligned} \tag{4.5}$$

where $n = (b-1)N + l$ with $l = 0, \ldots, N-1$; $b = K+1, \ldots, B$; $n = KN, \ldots, BN-1$ for steady state frame. Here, $\mathbf{x}_1$ is assumed to be cascade of B blocks of $\mathbf{x}_{1b}$ for $b = 1, \ldots, B$, i.e., $\mathbf{x}_1 = [\mathbf{x}_{11}, \mathbf{x}_{12}, \ldots, \mathbf{x}_{1b}]$ of size NB samples. (4.5) can be written in terms of $\mathbf{h}_1, \mathbf{h}_2$ and $\mathbf{h}_3$ as

$$y_1[n] = \sum_{k=0}^{K-1} x_{1(b-k)}[l]\, h_{k+1}[l], \tag{4.6}$$

where $h_{k+1}[l] = h[kN + l]$. For example shown in Fig. 4.2 with $K = 3$, steady state frame starts at $n = 3N$ corresponding to $b = 4$. For steady state frame, the autocorrelation of $\mathbf{y}_1$ is given by

$$\begin{aligned}
R_{y_1}(n, \tau) &= R_{y_1}((b-1)N + l, \tau) \\
&= E\{y_1[n]\, y_1^*[n+\tau]\} \\
&= E\Bigg\{\sum_{k=0}^{K-1}\sum_{m=0}^{K-1} y_{1(b-k)}[l+kN]\, y^*_{1(b-m)}[l+mN+\tau]\Bigg\} \\
&= \sum_{k=0}^{K-1}\sum_{m=0}^{K-1} E\{y_{1(b-k)}[l+kN]\, y^*_{1(b-m)}[l+mN+\tau]\} \\
&= \sum_{k=0}^{K-1} E\{y_{1(b-k)}[l+kN]\, y^*_{1(b-k)}[l+kN+\tau]\} \\
&= \begin{cases}
\frac{\sigma_s^2}{2}\sum_{k=0}^{K-1}\{h[l+kN]\cdot h[l+kN+\tau]\} & \tau = \pm pN \\
& \text{s.t. } KN \le n+\tau < BN \\
\\
0 & \text{Otherwise}
\end{cases},
\end{aligned} \tag{4.7}$$

for $p = 0, 1, \ldots, K-1$. Here the last but one step is due to the independence of data across different blocks, i.e., $E\{y_{1(b-k)}[l]\, y^*_{1(b-m)}[l+\tau] = 0$ for $k \neq m$ while the last step is due to (4.4). Note that the dependence of $R_{y_1}(n, \tau)$ on n is through l since $l = \text{mod}(n, N)$. For the example shown in the Fig. 4.2, we have for $n \in [3N, 4N-1]$,

$$R_{y_1}(n,\tau) = \begin{cases}
\frac{\sigma_s^2}{2}\Big(h_1^2[l] + h_2^2[l] + h_3^2[l]\Big) & \tau = 0 \\
\frac{\sigma_s^2}{2}\Big(h_1[l]\, h_2[l] + h_1[l]\, h_3[l]\Big) & \tau = \pm N \\
& \text{s.t. } 3N \le n+\tau < 7N \\
\frac{\sigma_s^2}{2}\Big(h_1[l]\, h_3[l]\Big) & \tau = \pm 2N \\
& \text{s.t. } 3N \le n+\tau < 7N \\
0 & \text{Otherwise}
\end{cases}, \tag{4.8}$$

for $l = \text{mod}(n, N)$. Fig. 4.3(c) shows the autocorrelation plot of $\mathbf{y}_1$ for various values of n and τ for $K = 3,\ N = 64$. The simulated values match well with theoretical values from (4.7). Observe that the autocorrelation values are non-zero for $\tau = 0, \pm N, \pm 2N$ for $K = 3$ although the values at the lag $\pm 2N$ are negligible as compared to those at the lags of 0 and $\pm N$.

4.2.5 Autocorrelation of Chain-2 output $y_2[n]$

The ACF for chain-2 can be derived similar to chain-1 as:

$$R_{y_2}(n,\tau) = \begin{cases} \frac{\sigma_s^2}{2}\sum_{k=0}^{K-1} h[l+kN-\frac{N}{2}]\cdot h[l+kN-\frac{N}{2}+\tau] & \tau = \pm pN \\ & \text{s.t. } KN \le n+\tau < BN \\ 0 & \text{Otherwise} \end{cases}, \tag{4.9}$$

for $l = \text{mod}(n, N)$, $n \in [KN, BN-1]$, and $p \in [0, K-1]$.

4.2.6 Autocorrelation of FBMC signal $y[n]$

At the last step, the output of chain-1 is added with the output of chain-2 delayed by $N/2$ samples, as shown in Fig. 4.2, so that

$$y[n] = y_1[n] + y_2[n-\frac{N}{2}]. \tag{4.10}$$

The ACF for $y[n]$ is given by

$$\begin{aligned} R_y(n,\tau) &= E\{y[n]y^*[n+\tau]\} \\ &= E\{(y_1[n]+y_2[n-\frac{N}{2}])(y_1[n+\tau]+y_2[n-\frac{N}{2}+\tau])^*\} \\ &= E\{y_1[n]y_1^*[n+\tau]\} + E\{y_2[n-\frac{N}{2}]y_2[n-\frac{N}{2}+\tau])^*\} \\ &= R_{y_1}(n,\tau) + R_{y_2}(n,\tau). \end{aligned} \tag{4.11}$$

The last step is from the fact that the output of the two chains are independent of each other and hence uncorrelated. Using (4.8) and (4.9) in (4.11), we get

$$R_y(n,\tau) = \begin{cases} \frac{\sigma_s^2}{2}\sum_{k=0}^{K-1}\{h[l+kN]\cdot h[l+kN+\tau] & \\ +h[l+kN-\frac{N}{2}]\cdot h[l+kN-\frac{N}{2}+\tau]\} & \tau = \pm pN \\ & \text{s.t. } KN \le n+\tau < BN \\ 0 & \text{Otherwise} \end{cases}. \tag{4.12}$$

Since $\mathbf{h}$ is a Nyquist pulse, we have [62, 66]

$$\begin{aligned} \sum_{k=0}^{K-1}\{h[l+kN]\,h[l+kN+\tau] + h[l+kN-\frac{N}{2}] \\ \cdot h[l+kN-\frac{N}{2}+\tau]\} = 0, \qquad \text{for } \tau \neq 0 \end{aligned}. \tag{4.13}$$

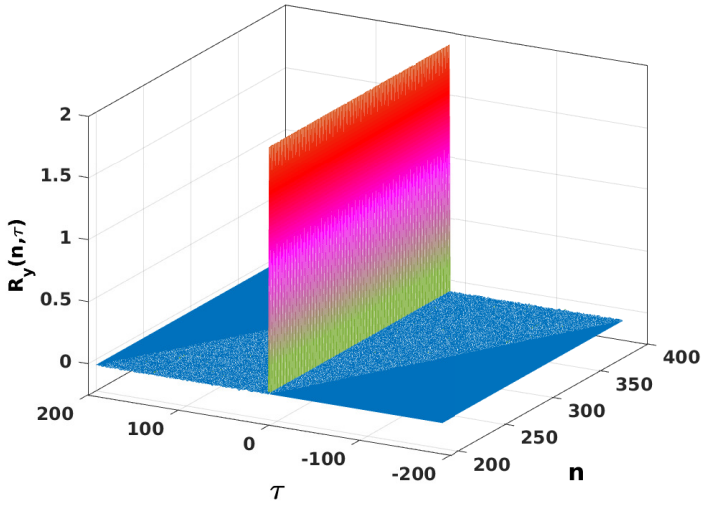

Figure 4.4: Simulated autocorrelation of the transmitted FBMC signal, $y[n]$ for $N = 64, K = 3$. The autocorrelation values are zero for non-zero lags. The number of Monte-Carlo realizations = 100000.

Using (4.13) in (4.12), we get

$$R_y(n,\tau) = \begin{cases} \frac{\sigma_s^2}{2} \sum_{k=0}^{K-1} \left(h^2[l+kN] + h^2[l+kN-\frac{N}{2}] \right) & \tau = 0 \\ 0 & \tau \neq 0 \end{cases}. \tag{4.14}$$

Fig. 4.4 shows the autocorrelation of $y[n]$ for different τ values for $K = 3,\ N = 64$. The autocorrelation value is non-zero for lag equal to zero and the value is zero for lag not equal to zero. The signal $y[n]$ exhibits no correlation property except for the zero-lag.

4.3 Proposed modification to the received FBMC signal and its autocorrelation analysis

Since the original received signal $y[n]$ does not have any correlation, the received signal needs to be modified. In this section, we discuss the modification of the FBMC signal at the receiver which will reveal the autocorrelation property. For convenience, we consider that the channel is noise-free in this section so that the transmitted as well as the received signals are same and denoted by $y[n]$. Note here that the received signal is processed (or modified) only at the receiver and not at the transmitter. Here, we only consider steady state part of frame so that $n \in [KN, BN-1]$. To simplify the notations, we use $t = n - KN$ such that $t \in [0, (B-K)N-1]$.

Section 4.2 shows that the autocorrelation existed for non-zero lags in the signal at various stages of FBMC signal generation and only at the last stage the autocorrelation at non-zero lags disappears

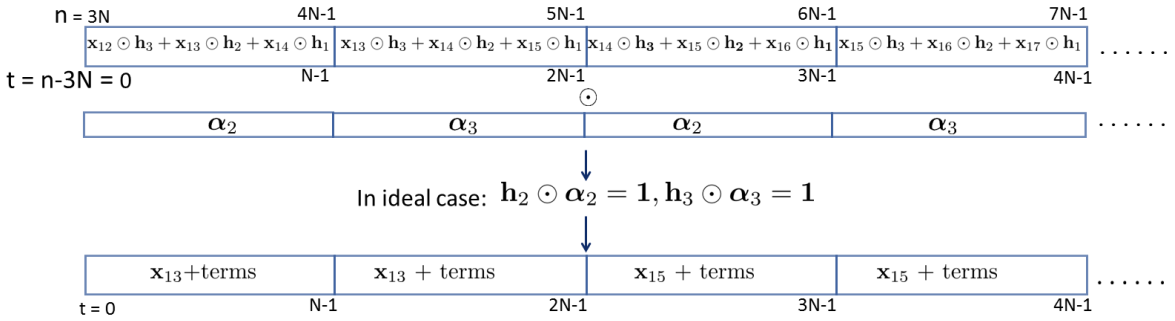

Figure 4.5: Four blocks from steady state frame of chain-1 section of $z[t]$. Idealized scenario which reveals correlation between samples at $\tau = N$. Steady state frame of chain-2 section of $z[t]$ is similar to that of chain-1 section and is not shown here. The samples of chain-2 of $z[t]$ are also correlated for $\tau = N$. The modification performed on $y[t]$ destroys the Nyquist pulse condition of $\mathbf{h}$ giving rise to non-zero correlation values of $z[t]$.

when the output of two chains are added. This happens due to the Nyquist property of the frequency-spreading-filter given by (4.13). We propose a modification to the received signal to get back the auto-correlation property.

Let $\boldsymbol{\alpha} = [\boldsymbol{\alpha_2}, \boldsymbol{\alpha_3}, \boldsymbol{\alpha_2}, \boldsymbol{\alpha_3}, \ldots, \boldsymbol{\alpha_2}, \boldsymbol{\alpha_3},]$ be a vector of length $(B-K)N$ where $\boldsymbol{\alpha}_2 = \mathbf{1} \oslash \mathbf{h}_2$ and $\boldsymbol{\alpha}_3 = \mathbf{1} \oslash \mathbf{h}_3$. Here, $\oslash$ denotes element-wise division. We denote the modified FBMC signal as $z[t]$ and it is given by

$$z[t] = z[n - KN] = z[(b - K - 1)N + l] = y[t]\alpha[t], \tag{4.15}$$

for $l \in [0, N-1]$.

To see how the proposed modification reveals autocorrelation property, look at the ideal scenario shown in Fig. 4.5 showing the output of chain-1 in steady state frame. If we multiply this output by $\boldsymbol{\alpha}$, that is the first block by $\boldsymbol{\alpha}_2$, second block by $\boldsymbol{\alpha}_3$, third block by $\boldsymbol{\alpha}_2$ and so on, then the resultant blocks of $\mathbf{z}$ have samples resulting in correlation as shown in Fig. 4.5. With this proposed modification to $z[t]$, the resultant samples of $z[t]$ produce non-zero autocorrelation values at lag N.

In practical implementations division by $\mathbf{h}$ is not possible as few indices of $\mathbf{h}$ containing very small values (tending to zero) will result in implementation issues such as autocorrelation values going to infinity. So, we modify the definition of $\boldsymbol{\alpha}_2$ and $\boldsymbol{\alpha}_3$ by introducing indicator function and a parameter δ such that

$$\alpha_2[l] = \frac{1}{h_2[l]} \cdot I_2(l, \delta) \text{ and } \alpha_3[l] = \frac{1}{h_3[l]} \cdot I_3(l, \delta), \tag{4.16}$$

where

$$I_2(l, \delta) = \begin{cases} 1 & h_2[l] > \delta \\ 0 & \text{otherwise} \end{cases} \text{ and } I_3(l, \delta) = \begin{cases} 1 & h_3[l] > \delta \\ 0 & \text{otherwise} \end{cases},$$

for $l \in [0, N-1]$. From Fig. 4.6, it is evident that autocorrelation function of modified FBMC signal,

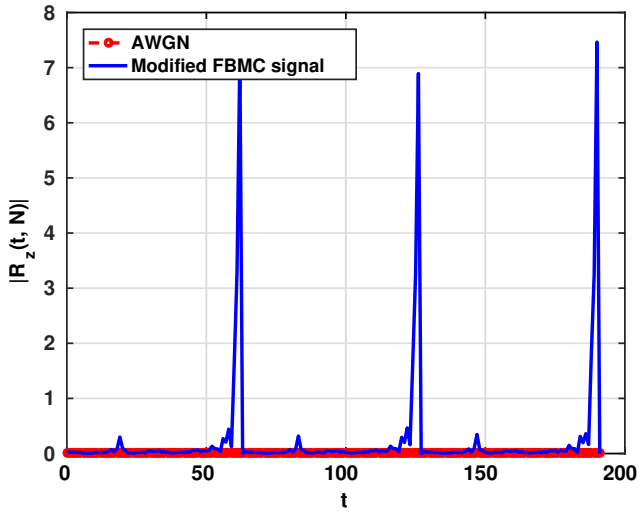

Figure 4.6: Simulated plot of $|R_z(t, N)|$. Here $N = 64$, the number of Monte-Carlo realizations = 10000. The correlation value at lag of N is non-zero for modified FBMC signal while the correlation is zero for AWGN samples.

$z[t]$, has non-zero values at lag of $\tau = N$. On the other hand, the AWGN samples, being independent, will not exhibit any autocorrelation property except at zero lag. Thus, this autocorrelation feature at lag of $\tau = N$ for the modified received FBMC signal is used to detect and differentiate between FBMC and noise signals.

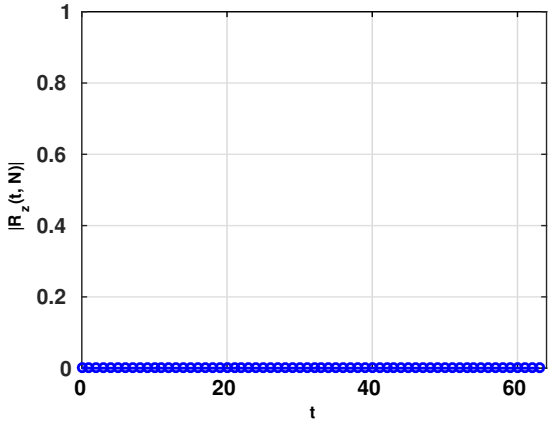

Figure 4.7: Simulated plot of $|R_z(t, N)|$ for $K = 2$. Here $N = 64$, the number of Monte-Carlo realizations = 10000. The correlation value at lag of N is zero even for modified FBMC signal.

$K = 2$: A special case

The autocorrelation value for $K = 2$ FBMC signal for $N = 64$ is shown in Fig. 4.7. The autocorrelation value is zero even after the proposed modification. The reason behind this result is explained below. The length of prototype filter for $K = 2$ and $N = 64$ is $KN = 128$. As stated earlier in the thesis that the prototype filter is divided in to K equal parts(2 parts in this case) for analysis purpose. Since, there are only two parts, say h_1 and h_2, and the impulse response of the filter being symmetric around $KN/2$, the division of received signal results in zero correlation as h_1 and h_2 cancel out each other due to symmetry.

Chapter 5

Autocorrelation-based detection of FBMC signal

Although blind detection techniques such as energy detection are used to detect any waveform, they cannot distinguish between noise and interfering signal. In addition, they have serious issues such as SNR walls [10]. Moreover, the ED does not consider the signal characteristics for spectrum sensing. Hence, they are not suitable to differentiate different primary signals. Also, parameter estimation of the primary signals is not possible as the blind detectors consider only the energy of the primary signals. As such, the need for feature based detectors has garnered much attention in the field of CR. Unlike blind detectors, feature based detectors use certain feature of the primary user waveform for spectrum sensing. For example, CP feature in OFDM signal. The feature present in the PU signal is used to estimate parameters of the waveform and hence to classify different PU signals. With this motivation for feature based detectors, we exploit the autocorrelation feature hidden in the FBMC signal for spectrum sensing of FBMC signal.

In this chapter, we present the design of an autocorrelation-based detector for sensing of FBMC signal. Next, We discuss the design of the detector using Neyman-Pearson criterion. Later, the performance of the proposed detector is examined under different scenarios such as timing offset, multipath channel model and noise uncertainty. Finally, the proposed detector's performance is compared with the performance of ED followed by combining the proposed detector with the ED.

5.1 Autocorrelation-based detection of FBMC signal

In this section, a detection scheme is presented to detect FBMC signal based on autocorrelation feature explored in sections 4.2 and 4.3. We begin by presenting the system model, followed by proposed test statistic. Next, we derive the distribution of the test statistic assuming Neyman-Pearson detection criterion.

The problem of detecting FBMC signal is modeled as a binary hypothesis testing problem. In our case, the binary hypothesis problem is to choose between the two hypotheses: H_0 (noise-only hypothesis) and H_1 (FBMC-signal-plus-noise hypothesis). If we denote the received signal in the presence of

AWGN as $v(t)$, then the two hypotheses will be given as

$$\begin{aligned} H_0: &\quad v[t] = w[t] \\ H_1: &\quad v[t] = y[t] + w[t]. \end{aligned} \tag{5.1}$$

However, the detection is done over the modified observations. Let the modified received signal is $u(t) = v(t)\alpha(t)$ so that the modified received signal under the two hypotheses is given as

$$\begin{aligned} H_0: &\quad u[t] = w[t]\alpha[t] \\ H_1: &\quad u[t] = (y[t] + w[t])\alpha[t] \\ &\qquad = z[t] + w'[t], \end{aligned} \tag{5.2}$$

where $w'[t] = w[t]\alpha[t]$, $w[t] \sim \mathcal{N}(0, \sigma_w^2)$ is the AWGN noise signal, $z[t] = y[t]\alpha[t]$ is the FBMC signal to be detected. In this thesis, the focus is on designing a detector which detects if the autocorrelation value at lag $\tau = N$ is zero or not. Note that the autocorrelation at other lags $\pm kN$ for $1 < k < K$ are negligible as compared to autocorrelation values at $\tau = N$ and have not been considered. In terms of ACF between the modified signal samples at lag $\tau = N$, the binary hypothesis test can be rewritten as

$$\begin{aligned} H_0: &\quad R_u(t, N) = R_{w'}(t, N) = 0 \\ H_1: &\quad R_u(t, N) = R_z(t, N) + R_{w'}(t, N) = R_z(t, N) \neq 0. \end{aligned} \tag{5.3}$$

For this binary hypothesis test, the proposed test statistic T_A is

$$T_A = \sum_{t=0}^{N-1} \frac{|\hat{R}_u(t, N)|^2}{\sigma_{rt}^2}, \tag{5.4}$$

where $\hat{R}_u(t, N)$ is the maximum likelihood estimate of $R_u(t, N)$ based on the observations and is given by

$$\hat{R}_u(t, N) = \frac{1}{N_f} \Re\left\{ \sum_{n_f=0}^{N_f-1} u[t + n_f N] u^*[t + n_f N + N] \right\}, \tag{5.5}$$

and σ_{rt}^2 is the variance of $\hat{R}_u(t, N)$ under H_0 hypothesis, N_f ($\leq B - K$) is total number of data blocks present in the steady-state frame of FBMC signal. Here, $\Re\{.\}$ represents real part of a complex signal. The proposed test statistic T_A is the weighted sum of squares of the estimated autocorrelation values. The weights $\frac{1}{\sigma_{rt}^2}$ normalizes any noise amplification because of multiplication with $\alpha(t)$. Moreover, the test statistic does not need any information regarding FBMC signal except N, which is generally available in standards.

We employ Neyman-Pearson detection criterion that maximizes the probability of detection for a given false alarm rate so that H_1 is decided if $T_A > \gamma$. Now we need to derive the distribution of T_A under H_0, which depends on the distribution of $\hat{R}_u(t, N)$.

5.1.1 Distribution of $\hat{R}_u(t,N)$ under H_0

Employing central limit theorem for sufficiently large N_f in (5.5), we can approximate $\hat{R}_u(t,N)$ as a Gaussian random variable. The mean of $\hat{R}_u(t,N)$ under H_0 hypothesis is given by

$$E[\hat{R}_u(t,N)|H_0] = E\left\{\frac{1}{N_f}\sum_{n_f=0}^{N_f-1} u[t+n_fN]u^*[t+n_fN+N]\right\}. \tag{5.6}$$

Under H_0, $u[t] = w'[t] = w[t]\alpha[t]$. So,

$$\begin{aligned} E[\hat{R}_u(t,N)|H_0] &= E\left\{\frac{1}{N_f}\sum_{n_f=0}^{N_f-1} w[t+n_fN]\alpha[t+n_fN]w^*[t+n_fN+N]\alpha^*[t+n_fN+N]\right\} \\ &= \frac{1}{N_f}\sum_{n_f=0}^{N_f-1} E\left\{w[t+n_fN]w^*[t+n_fN+N]\alpha[t+n_fN]\alpha[t+n_fN+N]\right\} \\ &= 0, \end{aligned} \tag{5.7}$$

since noise values are uncorrelated for $\tau = N$. As $\alpha[t]$ is a real quantity, we use $\alpha^*[t] = \alpha[t]$ in subsequent equations. If S is a circularly symmetric complex Gaussian random variable having variance σ^2 then $\Re\{S\}$ will also be a Gaussian random variable with variance $\frac{\sigma^2}{2}$. Variance of $\hat{R}_u(t,N)$ is given by

$$\text{Var}(\hat{R}_u(t,N)\,|\,H_0) = \frac{E[\hat{R}_u^2(t,N)\,|\,H_0] - E^2[\hat{R}_u(t,N)\,|\,H_0]}{2}. \tag{5.8}$$

Now,

$$\begin{aligned} E[\hat{R}_u^2(t,N)\,|\,H_0] &= E\left\{\left(\frac{1}{N_f}\sum_{n_f=0}^{N_f-1} w[t+n_fN]\alpha[t+n_fN]w^*[t+n_fN+N]\alpha[t+n_fN+N]\right)^2\right\} \\ &= \frac{1}{N_f^2}E\left\{\sum_{n_{f_1}=0}^{N_f-1}\sum_{n_{f_2}=0}^{N_f-1} w[t+n_{f_1}N]\alpha[t+n_{f_1}N]\right. \\ &\quad w^*[t+n_{f_1}N+N]\alpha[t+n_{f_1}N+N]w[t+n_{f_2}N] \\ &\quad \left.\alpha[t+n_{f_2}N]w^*[t+n_{f_2}N+N]\alpha[t+n_{f_2}N+N]\right\}. \end{aligned} \tag{5.9}$$

If $A,\ B,\ C,\ D$ are jointly Gaussian random variables then from [67]

$$E\{ABCD\} = E\{AB\}E\{CD\} + E\{AC\}E\{BD\} + E\{AD\}E\{BC\} - 2E\{A\}E\{B\}E\{C\}E\{D\}. \tag{5.10}$$

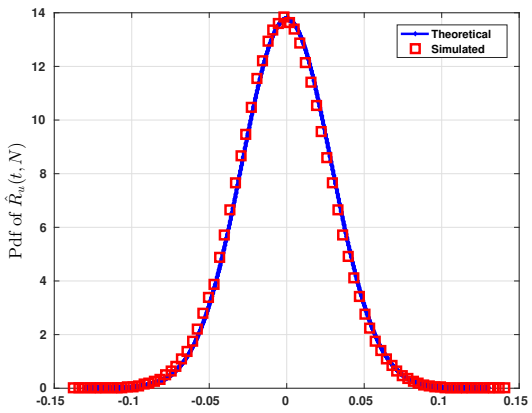

Figure 5.1: The theoretical and simulated pdf of $\hat{R}_u(t,N)$ under H_0 for $N = 64, K = 3, \delta = 0.001$ while the number of Monte-Carlo realizations = 100000. The theoretical and simulated pdf match well.

Using (5.10) in (5.9), we get

$$E[\hat{R}_u^2(t,N)|H_0] = \begin{cases} \sum_{n_f=0}^{N_f-1} \frac{\alpha^2[t+n_fN]\alpha^2[t+n_fN+N](\sigma_w^2)^2}{N_f^2} & ; n_{f_1} = n_{f_2} \\ 0 & ; n_{f_1} \neq n_{f_2} \end{cases}. \tag{5.11}$$

Substituting (5.7), (5.11) in (5.8), we get

$$\text{Var}\{\hat{R}_u(t,N) \mid H_0\} = \sum_{n_f=0}^{N_f-1} \frac{\alpha^2[t+n_fN]\alpha^2[t+n_fN+N](\sigma_w^2)^2}{2N_f^2}. \tag{5.12}$$

Hence, the distribution of $\hat{R}_u(t,N)$ under H_0 is given as

$$\hat{R}_u(t,N) \sim \mathcal{N}(0, \sigma_{rt}^2), \tag{5.13}$$

where

$$\sigma_{rt}^2 = \sum_{n_f=0}^{N_f-1} \frac{\alpha^2[t+n_fN]\alpha^2[t+n_fN+N](\sigma_w^2)^2}{2N_f^2}. \tag{5.14}$$

Fig. 5.1 shows the theoretical and simulated probability density function (pdf) of $\hat{R}_u(t,N)$. It can be seen that both the curves match very well. Now, the correlation between $\hat{R}_u(t_1,N)$ and $\hat{R}_u(t_2,N)$ is

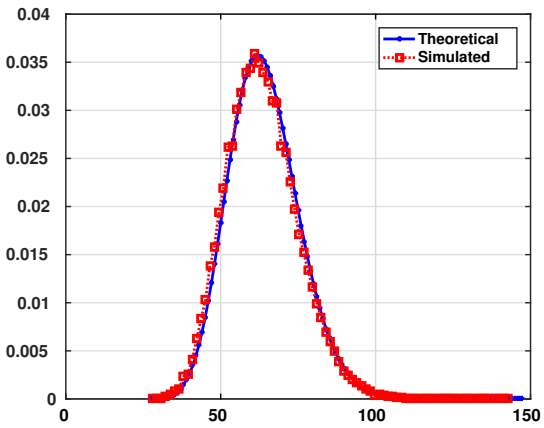

Figure 5.2: The theoretical and simulated pdf of T_A under H_0 for $N = 64, K = 3, \delta = 0.001$ while the number of Monte-Carlo realizations = 100000.

given by

$$E\{\hat{R}_u(t_1,N)\cdot\hat{R}_u(t_2,N)\,|\,H_0\} = E\Big\{\big(\frac{1}{N_f}\sum_{n_{f1}=0}^{N_f-1} w[t_1+n_{f1}N]\,\alpha[t_1+n_{f1}N]$$
$$w^*[t_1+n_{f1}N+N]\,\alpha^*[t_1+n_{f1}N+N]\big)$$
$$\cdot\big(\frac{1}{N_f}\sum_{n_{f2}=0}^{N_f-1} w[t_2+n_{f2}N]\,\alpha[t_2+n_{f2}N]$$
$$w^*[t_2+n_{f2}N+N]\alpha^*[t_2+n_{f2}N+N]\big)\Big\}.$$

Using (5.10) along with independence of $w[t_1]$ and $w[t_2]$ for $t_1 \neq t_2$, we get

$$E\{\hat{R}_u(t_1,N)\cdot\hat{R}_u(t_2,N)\,|\,H_0\} = 0. \tag{5.15}$$

Under H_0, $\hat{R}_u(t,N)/\sigma_{rt}$ has a standard Gaussian distribution from (5.13) while $\hat{R}_u(t_1,N)$ and $\hat{R}_u(t_2,N)$ are uncorrelated for $t_1 \neq t_2$ from (5.15). This means that $\hat{R}_u(t,N)$ are IID Gaussian random variables for different values of t.

5.1.2 Distribution of T_A under H_0

The test statistic T_A is sum of squares of N IID standard Gaussian random variables $\hat{R}_u(t,N)/\sigma_{rt}$ and therefore will follow central Chi-Square distribution with N degrees of freedom under H_0 as shown in Fig. 5.2. Therefore, P_{FA} is given [40] by

$$P_{FA} = Pr\{T_A > \gamma\,|\,H_0\} = Q_{\chi^2_N}(\gamma), \tag{5.16}$$

where $Q_{\chi^2_N}$ is the right tail probability for a Chi-Square random variable. The threshold γ for the Neyman-Pearson detector is given by

$$\gamma = Q^{-1}_{\chi^2_N}(P_{FA}). \tag{5.17}$$

5.2 Results

In this section, we present the proposed detector's performance in terms of P_D Vs SNR curves and receiver operating characteristics (ROC) for different values of N and K. This will be followed by the effects of δ on the detection performance. Next, the assumption of frame synchronization (in terms of time) is relaxed to show that the performance does not change with loss of time-offset. Later, the detector's performance under multipath scenario and noise uncertainty is presented. Finally, we compare the performance of our detector with traditional ED. The detection scheme is designed based on

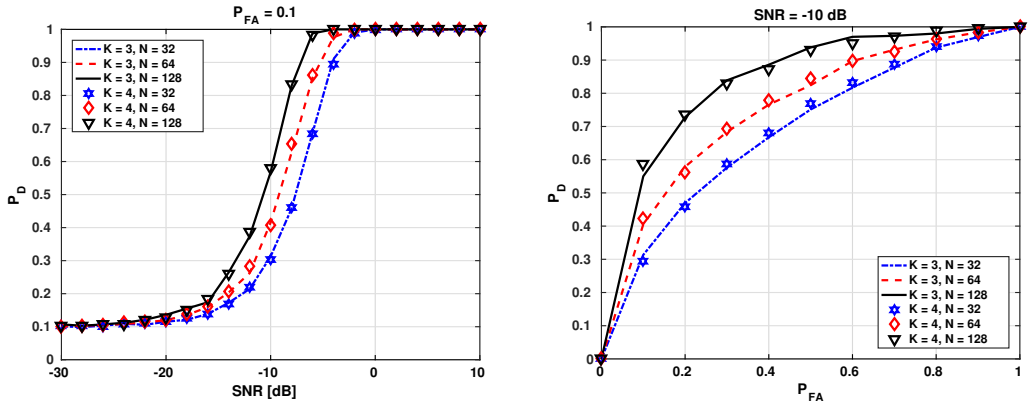

(a) P_D Vs SNR (dB)

(b) Receiver operating characteristics (ROC)

Figure 5.3: Probability of detection and ROC curves for the proposed autocorrelation based detector with various K and N values. Here number of Monte-Carlo realizations is 5000, while number of blocks is 100.

Neyman-Pearson detection criterion with $P_{FA} = 0.1$. All the simulations are performed on MATLAB with the following parameters unless specified otherwise: $K = 3$, $N = 64$, number of FBMC blocks in steady state $N_f = 100$, $\tau = N$. The detection is performed assuming that noise power is known. SNR [dB] is defined as $10\log(\frac{\sigma_y^2}{\sigma_w^2})$.

5.2.1 Detection performance for different K and N

Fig. 5.3(a) presents P_D Vs SNR [dB] curves for $P_{FA} = 0.1$ while Fig. 5.3(b) shows ROC for SNR $= -10$ dB for different values of K(=3, 4) and N(=32, 64, 128). From both the figures, it is evident that the detector has good performance for different values of N and K. The detector has good performance even for the low SNR values. Performance of the detector improves going from $N = 32$ to 128 because

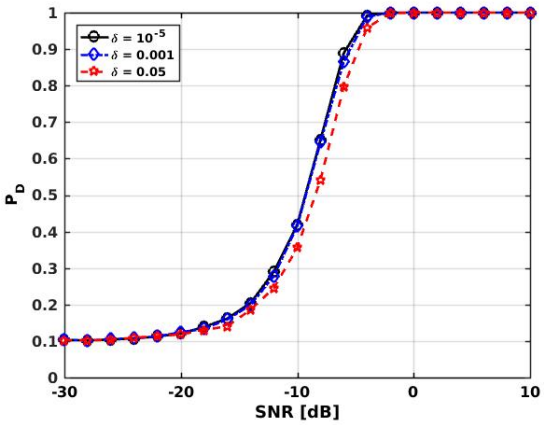

Figure 5.4: P_D Vs SNR [dB] plot of FBMC signal for different values of δ with $N = 64, K = 3, P_{FA} = 0.1$. Here number of Monte-Carlo realizations is 5000 while number of blocks is 100. The performance of the detector degrades slightly with increase in δ value after $\delta > 0.001$ in the considered scenario.

of increase in number of samples. On the other hand, there is hardly any improvement when $K = 4$ is used instead of $K = 3$ as number of samples hardly change.

The threshold for the detector has been set empirically for $P_{FA} = 0.1$. From Fig. 5.3(a), it is evident that the detector maintains $P_{FA} = 0.1$ under extremely low SNR values ($< -30dB$), which is equivalent H_0.

5.2.2 Effect of δ on the detector performance

Fig. 5.4 shows the P_D vs SNR curves for different values of δ (parameter associated with indicator function used for division) with $K = 3, N = 64, P_{FA} = 0.1$. Here number of Monte-Carlo realizations is 5000 while number of blocks is 100. It can be inferred from the figure that the detection performance is almost similar for $\delta \leq 0.001$. However, for large values of $\delta > 0.001$, there is slight degradation which will increase with increase in the value of δ. This is expected, because as δ increases, more number of samples of $z[t]$ become zero and the number of non-zero samples contributing to the detection decreases. However, for low value of $\delta \leq 0.001$, the number of samples going to zero is very few.

5.2.3 Effect of timing offset on the detector performance

So far, the detection of FBMC signal is performed assuming both the transmitter and the receiver are perfectly synchronized. However, this assumption is unrealistic given that for synchronization we first need to know whether the signal is present or not. Thus considering the effect of timing offset is important which is the focus of this subsection. Fig. 5.5 shows different timing offset considered and their effect as data-blocks will be multiplied by shifted versions of $\boldsymbol{\alpha}_2$ and $\boldsymbol{\alpha}_3$. Fig. 5.6(a) shows the proposed detector's performance in the presence of different values of time-offset ϵ which is unknown

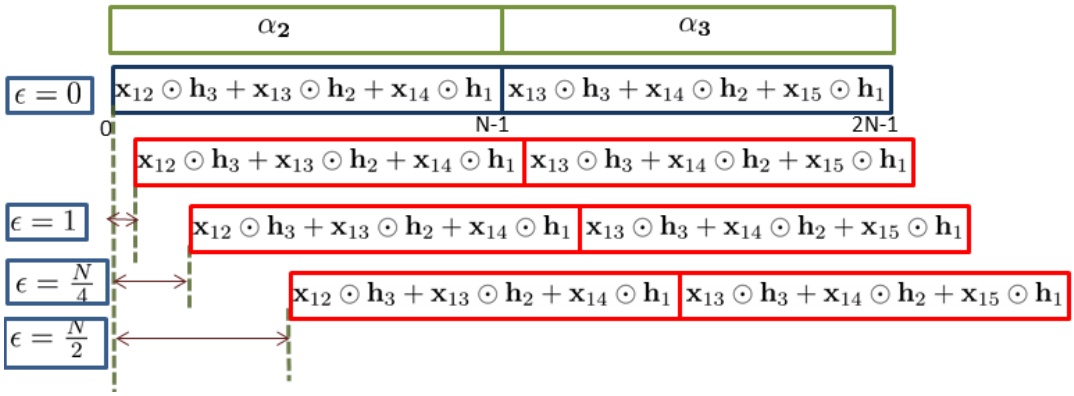

Figure 5.5: Scenarios with different timing offsets ϵ between the received signal and the vector $\boldsymbol{\alpha}$. With the non-zero offset present, coefficients $\boldsymbol{\alpha}$ are being multiplied by delayed FBMC samples by the respective offset.

at the receiver. The simulation parameters are $N = 64, K = 3$, and $P_{FA} = 0.1$ with number of Monte-Carlo realizations 5000. The number of steady-state blocks is $N_f = 100$ which corresponds to 6400 samples. It can be seen from the figure that there is hardly any change in the performance of the autocorrelation based detector even in the absence of timing synchronization. To understand why the timing offset does not affect the detector's performance, we simulated the mean and variance of the test statistic in the presence of offset ϵ, denoted by $T(\epsilon)$, under the alternative hypothesis. Fig. 5.6(b) shows the simulated mean and variance for $T(\epsilon)$ under H_1 for SNR $= -10$ dB as a function of ϵ. It can be observed from Fig. 5.6(b) that the mean and variance of the proposed test statistic $T(\epsilon)$ under H_1 are almost constant irrespective of ϵ. Thereby the detection performance of the detector doesn't change much with the timing offset.

5.2.4 Detection of FBMC signal under multipath Scenario

Thus far, we considered AWGN channel model for simplicity. However, in reality channels are modeled to be multipath Rayleigh fading channels. In this section, we evaluate the behavior of the detector in multipath environment. Let P be the order of a multipath channel and $g[l]$ represent channel coefficients for $l = 0, 1, \ldots P-1$. Now, the received signal under H_1 hypothesis in multipath scenario is given as:

$$\begin{aligned} H_1: \quad u[t] &= \big(g[t] \star y[t]\big)\alpha[t] + w'[t] \\ &= \left(\sum_{l=0}^{P-1} g[l]y[t-l]\right)\alpha[t] + w'[t], \end{aligned} \tag{5.18}$$

where $\star$ denotes convolution. We use (5.18) to simulate P_D values empirically. Fig. 5.7 shows the P_D Vs SNR curve for both AWGN and multipath channel models. Observe that the detector performs better for AWGN channel model because AWGN channel being the simple model with only single tap between the

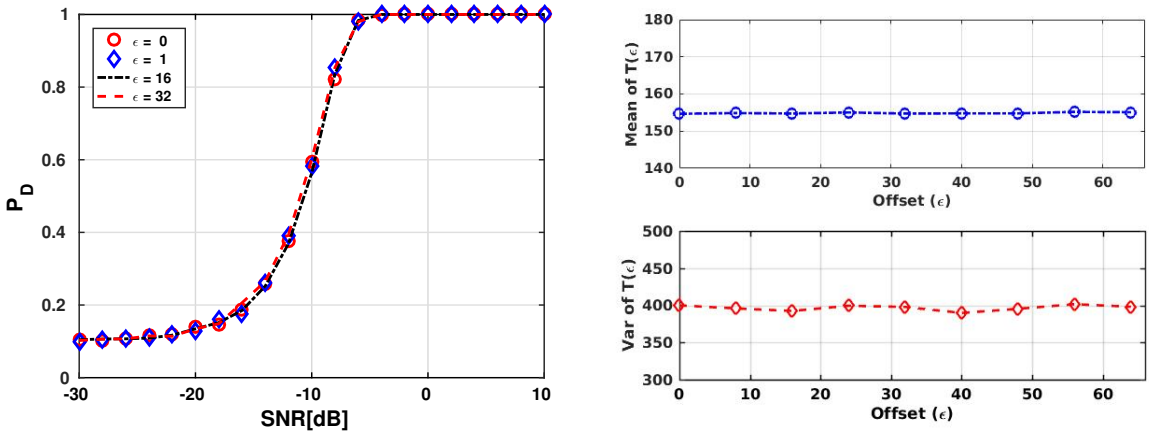

(a) (b)

Figure 5.6: P_D Vs SNR curve for different offsets. The proposed detector performs well irrespective of timing offsets. (b) Mean and variance of Test statistic, $T(\epsilon)$, for different offsets under H_1 hypothesis. Here, $K = 3, N = 64, \delta = 0.001$, SNR=$-10$ dB, and $N_f = 100$. It can be inferred that the mean and variance of $T(\epsilon)$ are independent of offset. Number of Monte-Carlo realizations=5000.

transmitter and the receiver. At the other hand, for the multipath model with a line of sight (LOS) path and several non LOS paths, the received signal will be addition of LOS and non LOS paths accounting to either constructive interference or destructive interference at the receiver. Hence, in general, the detector's performance for multipath scenario degrades. However, the performance degradation of the proposed detector is very much less. It is noticeable that the proposed autocorrelation based detector is robust to multipath channel models too.

5.2.5 Effect of noise uncertainty

Thus far, the results presented are under the assumption that noise variance is known. However, perfect knowledge of noise power is not available in practical scenarios and there exists some uncertainty in noise power [10]. Let the noise uncertainty is distributed as $\sigma_u^2 \in [(1/\psi)\hat{\sigma}_w^2,\ \psi\hat{\sigma}_w^2]$. Here, $\hat{\sigma}_w^2$ is expected or average noise power and ψ (> 1) is known as uncertainty parameter. The noise uncertainty is expressed as $\Delta = 10\log_{10}\psi$ in dB or $\psi = 10^{\Delta/10}$. In this work, the noise uncertainty considered is 0.5 dB. The noise is considered to be an unknown constant. From Fig. 5.8, it is evident that the performance of both the detectors degrade considerably, the degradation is much more severe in the ED. Hence, the proposed detector performs better compared to the ED under noise uncertainty.

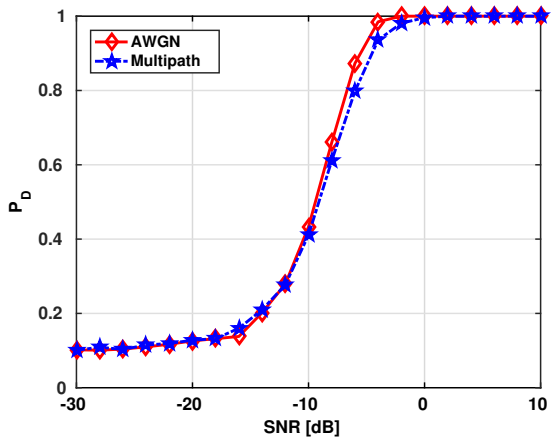

Figure 5.7: P_D Vs SNR curve for multipath scenario. The detector performance is shown for both AWGN and multipath channel scenarios. Performance of the detector under multipath scenario is very much close to that of AWGN case.

5.2.6 Comparison and cooperation with energy detector

Fig. 5.9 shows the comparison between the classical ED and the proposed autocorrelation detector's performance. Here, the test statistic for the ED, T_E, is given [40] by

$$T_E = \sum_{t=0}^{N_f N-1} |v[t]|^2. \tag{5.19}$$

It is inferred from the figure that the ED outperforms the proposed detector. It is expected as the ED is the optimal detector when detecting a random signal in noise with the noise variance is perfectly known. However, note that the ED is a blind detector and cannot distinguish target signal from the noise or any interference. The proposed detector on the other hand can distinguish between FBMC signal and noise. It can also differentiate between different FBMC signals which have different values of N. The two detectors can also be combined to improve the detection performance. Since both T_A and T_E are evaluated from the same data, there may be some correlation between the test statistics under both the hypothesis. Therefore, the test statistic for the cooperative scenario is considered as [40]

$$T_{\text{comb}} = \begin{bmatrix} T_E & T_A \end{bmatrix} \begin{bmatrix} \sigma_E^2 & \rho\,\sigma_E\,\sigma_A \\ \rho\,\sigma_E\,\sigma_A & \sigma_A^2 \end{bmatrix} \begin{bmatrix} T_E \\ T_A \end{bmatrix}, \tag{5.20}$$

with ρ being the correlation coefficient between T_E and T_A while σ_E^2 and σ_A^2 corresponds to variance of T_E and T_A, respectively, all under the null hypothesis. The threshold for this case has been obtained empirically. Fig. 5.9 also shows P_D Vs SNR curve for the combined detector for $N = 64, K = 3$, $\delta = 0.001$ and number of realizations is 5000. A noticeable improvement is visible in the detection performance when the two detectors cooperate as compared to their individual performance.

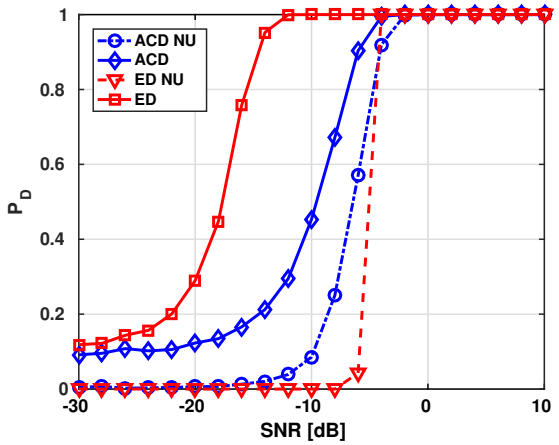

Figure 5.8: P_D Vs SNR plot of ED and the proposed autocorrelation based detector under noise uncertainty (NU) of 0.5 dB. Here, $K = 3,\ N = 64, \delta = 0.001$ and $N_f = 100$. The performance of both the detectors is affected by uncertainty in noise. However, there is a drastic degradation in performance in case of ED.

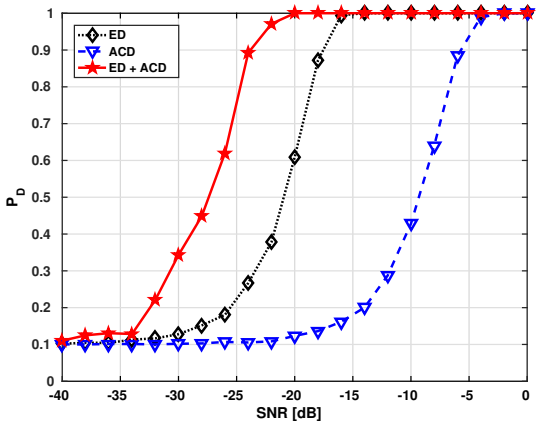

Figure 5.9: P_D Vs SNR plot of combined detector of FBMC signal for $K = 3,\ N = 64, \delta = 0.001$ and $N_f = 100$. Number of Monte-Carlo realizations = 5000. It can be inferred that the combination of proposed autocorrelation detector and ED improves overall detection performance.

Chapter 6

Conclusions and Future scope

6.1 Conclusions

FBMC signal is considered as a suitable candidate waveform for 5G to enhance the spectral efficiency and provide high data rates. In this thesis, FBMC signal is studied extensively with more attention being given to FBMC signal generation and its structure. FBMC signal is properly analyzed and it is found that there is an autocorrelation property among the FBMC samples. However, the autocorrelation property vanishes at the last stage of FBMC signal generation. A suitable modification is proposed to the received FBMC signal to retrieve the autocorrelation value of FBMC signal. It is shown that the proposed modification gives non-zero autocorrelation values for a lag equal to the number of subcarriers. The non-zero autocorrelation values are used to design a feature detector.

An autocorrelation based detector is designed to detect FBMC signal in the presence of noise. The non-zero autocorrelation value obtained after the modification is used to design the detector. The key idea used here is that the noise samples being uncorrelated for lags other than zero gives zero correlation values whereas FBMC samples are correlated for a lag equal to the number of subcarriers. A Neyman-Pearson detector is modeled that maximizes detection probability while maintaining a constant probability of false alarm. The proposed detector is designed based on the autocorrelation property of the FBMC signal. The threshold for the detection is obtained under the null hypothesis and the test statistics for the proposed detector is compared with the threshold to decide presence or absence of FBMC signal.

The proposed detector has a good detection performance even in low SNR regimes. The detector's performance has been analyzed under different non-idealities like multipath fading channel model, noise uncertainty and no frame synchronization. We conclude that the proposed autocorrelation based detector is very much robust to these non-idealities. The proposed detector is combined with the energy detector to increase the over all detection performance.

6.2 Scope for future work

This research work can be extended based on the following ideas:

1. The detector designed in this thesis is used for local spectrum sensing by a SU. However, in fading scenarios it is always suggested to perform cooperative spectrum sensing to obtain better sensing results to decide presence or absence of PU. In this regard, the proposed detector can be extended to cooperative scenario both for homogeneous and heterogeneous sensors.

2. It is proved in this work that FBMC signal has inherent autocorrelation property. Cepstrum tool may be applied to separate the data samples from the filter coefficients making use of autocorrelation property.

3. This work can further be extended to estimate several key parameters of the received FBMC signal such as number of subcarriers in the signal, the overlapping factor used etc.

Related Publications

1. Upender Keesara and Sachin Chaudhari, Autocorrelation-Based Spectrum Sensing of FBMC Signal, in *Proc. 10th International Conference on Communication Systems and Networks (COMSNETS)*, January 2018.

2. Upender Keesara and Sachin Chaudhari, Autocorrelation-Based Spectrum Sensing of FBMC Signals in Cognitive Radios, submitted to *Elsevier Physical Communication Journal.*

Bibliography

[1] A. Gupta and R. K. Jha, "A survey of 5G network: Architecture and emerging technologies," *IEEE Access*, vol. 3, pp. 1206–1232, 2015.

[2] G. Wunder *et al.*, "5GNOW: non-orthogonal, asynchronous waveforms for future mobile applications," *IEEE Communications Magazine*, vol. 52, no. 2, pp. 97–105, February 2014.

[3] P. K. Agyapong, M. Iwamura, D. Staehle, W. Kiess, and A. Benjebbour, "Design considerations for a 5G network architecture," *IEEE Communications Magazine*, vol. 52, no. 11, pp. 65–75, 2014.

[4] B. Farhang-Boroujeny, "OFDM versus filter bank multicarrier," *IEEE Signal Processing Magazine*, vol. 28, no. 3, pp. 92–112, May 2011.

[5] ——, "Filter bank multicarrier modulation: A waveform candidate for 5G and beyond," *Advances in Electrical Engineering*, vol. 2014, 2014.

[6] J. B. Dore, R. Gerzaguet, N. Cassiau, and D. Ktenas, "Waveform contenders for 5G: Description, analysis and comparison," *Physical Communication*, vol. 24, no. Supplement C, pp. 46 – 61, 2017.

[7] Y. Liu, X. Chen, Zhong *et al.*, "Waveform candidates for 5G networks: Analysis and comparison," *arXiv:1609.02427*, 2016.

[8] P. Banelli *et al.*, "Modulation formats and waveforms for 5G networks: Who will be the heir of OFDM?: An overview of alternative modulation schemes for improved spectral efficiency," *IEEE Signal Processing Magazine*, vol. 31, no. 6, pp. 80–93, 2014.

[9] S. Chaudhari, "Spectrum sensing for cognitive radios: Algorithms, performance and limitations," Ph.D. dissertation, Aalto University School of Electrical Engineering, Nov. 2012.

[10] R. Tandra and A. Sahai, "SNR Walls for Signal Detection," *IEEE J. of Sel. Topics in Signal Process.*, vol. 2, no. 1, pp. 4–17, 2008.

[11] H. Zhang, D. Le Ruyet, and M. Terré, "Spectral correlation of multicarrier modulated signals and its application for signal detection," *EURASIP Journal on Advances in Signal Processing*, vol. 2010, no. 1, p. 1, 2009.

[12] D. Evans, "The internet of things: How the next evolution of the internet is changing everything," *CISCO white paper*, vol. 1, pp. 1–11, 2011.

[13] A. Ijaz *et al.*, "Enabling massive IoT in 5G and beyond systems: PHY radio frame design considerations," *IEEE Access*, vol. 4, pp. 3322–3339, 2016.

[14] Y. Kishiyama, A. Benjebbour, T. Nakamura, and H. Ishii, "Future steps of LTE-A: evolution toward integration of local area and wide area systems," *IEEE Wireless Communications*, vol. 20, no. 1, pp. 12–18, 2013.

[15] E. Hossain and M. Hasan, "5G cellular: key enabling technologies and research challenges," *IEEE Instrumentation & Measurement Magazine*, vol. 18, no. 3, pp. 11–21, 2015.

[16] G. P. Fettweis, "A 5G wireless communications vision," *Microwave Journal*, vol. 55, no. 12, pp. 24–36, 2012.

[17] A. Osseiran *et al.*, "Scenarios for 5G mobile and wireless communications: the vision of the METIS project," *IEEE Communications Magazine*, vol. 52, no. 5, pp. 26–35, 2014.

[18] H. Kim, "Coding and modulation techniques for high spectral efficiency transmission in 5G and satcom," in *2015 IEEE 23rd European Signal Processing Conference (EUSIPCO)*. IEEE, 2015, pp. 2746–2750.

[19] M. Sybis, K. Wesolowski, K. Jayasinghe, V. Venkatasubramanian, and V. Vukadinovic, "Channel coding for ultra-reliable low-latency communication in 5G systems," in *2016 IEEE 84th Vehicular Technology Conference (VTC-Fall)*. IEEE, 2016, pp. 1–5.

[20] A. Benjebbour *et al.*, "System-level performance of downlink NOMA for future LTE enhancements," in *2013 IEEE Globecom Workshops*. IEEE, 2013, pp. 66–70.

[21] E. G. Larsson, O. Edfors, F. Tufvesson, and T. L. Marzetta, "Massive MIMO for next generation wireless systems," *IEEE communications magazine*, vol. 52, no. 2, pp. 186–195, 2014.

[22] Y. H. Nam *et al.*, "Full-dimension MIMO (FD-MIMO) for next generation cellular technology," *IEEE Communications Magazine*, vol. 51, no. 6, pp. 172–179, 2013.

[23] L. Song, M. Peng, and Y. Li, "Resource allocation for vertical sectorization in LTE-advanced systems," *International Journal of Antennas and Propagation*, 2013.

[24] T. S. Rappaport *et al.*, "Millimeter wave mobile communications for 5G cellular: It will work!" *IEEE access*, vol. 1, pp. 335–349, 2013.

[25] Z. Pi and F. Khan, "An introduction to millimeter-wave mobile broadband systems," *IEEE communications magazine*, vol. 49, no. 6, 2011.

[26] J. F. Gomes, P. Ahokangas, and S. Moqaddamerad, "Business modeling options for distributed network functions virtualization: Operator perspective," in *Proceedings of 2016 22nd European Wireless Conference*. VDE, 2016, pp. 1–6.

[27] C.-I. Badoi, N. Prasad, V. Croitoru, and R. Prasad, "5G based on cognitive radio," *Wireless Personal Communications*, vol. 57, no. 3, pp. 441–464, 2011.

[28] FCC, "FCC notice of proposed rule making and order: Facilitating opportunities for flexible, efficient, and reliable spectrum use employing cognitive radio technologies ET Docket No. 03-108," Feb, 2005.

[29] S. Geirhofer, L. Tong, and B. M. Sadler, "Cognitive radios for dynamic spectrum access-dynamic spectrum access in the time domain: Modeling and exploiting white space," *IEEE Communications Magazine*, vol. 45, no. 5, 2007.

[30] Q. Zhao and B. M. Sadler, "A survey of dynamic spectrum access," *IEEE signal processing magazine*, vol. 24, no. 3, pp. 79–89, 2007.

[31] T. Yucek and H. Arslan, "A survey of spectrum sensing algorithms for cognitive radio applications," *IEEE communications surveys & tutorials*, vol. 11, no. 1, pp. 116–130, 2009.

[32] I. F. Akyildiz, W.-Y. Lee, M. C. Vuran, and S. Mohanty, "A survey on spectrum management in cognitive radio networks," *IEEE Communications magazine*, vol. 46, no. 4, 2008.

[33] E. Hossain, M. Rasti, H. Tabassum, and A. Abdelnasser, "Evolution toward 5G multi-tier cellular wireless networks: An interference management perspective," *IEEE Wireless Communications*, vol. 21, no. 3, pp. 118–127, 2014.

[34] N. Saquib, E. Hossain, L. B. Le, and D. I. Kim, "Interference management in OFDMA femtocell networks: Issues and approaches," *IEEE Wireless Communications*, vol. 19, no. 3, 2012.

[35] B. Gao, J.-M. Park, Y. Yang, and S. Roy, "A taxonomy of coexistence mechanisms for heterogeneous cognitive radio networks operating in TV white spaces," *IEEE Wireless Communications*, vol. 19, no. 4, 2012.

[36] M. Pucci, "Interference management in next generation wireless systems: Cognitive and coordinated approaches," 2014.

[37] V. Marojevic, J. Salazar, X. Revés, and A. Gelonch, "On integrating radio, computing, and application resource management in cognitive radio systems," in *2007 Third IEEE International Conference on Wireless and Mobile Computing, Networking and Communications (WiMOB 2007)*, pp. 32–32.

[38] N. Hoven and A. Sahai, "Power scaling for cognitive radio," in *2005 International Conference on Wireless networks, communications and mobile computing,*, vol. 1. IEEE, 2005, pp. 250–255.

[39] X. Jing, S.-C. Mau, D. Raychaudhuri, and R. Matyas, "Reactive cognitive radio algorithms for co-existence between IEEE 802.11 b and 802.16 a networks," in *2005 Global Telecommunications Conference (GLOBECOM'05)*, vol. 5. IEEE, 2005, pp. 5–pp.

[40] S. Kay, *Fundamentals of Statistical Signal Processing: Volume II Detection Theory*. Prentice Hall, 1998.

[41] R. Umar and A. U. Sheikh, "A comparative study of spectrum awareness techniques for cognitive radio oriented wireless networks," *Physical Communication*, vol. 9, pp. 148–170, 2013.

[42] S. J. Shellhammer, "A comparison of geo-location and spectrum sensing in cognitive radio," in *Proceedings of 2009 18th Internatonal Conference on Computer Communications and Networks (ICCCN)*. IEEE, 2009, pp. 1–6.

[43] A. Hulbert, "Spectrum sharing through beacons," in *IEEE 2005 16th International Symposium on Personal, Indoor and Mobile Radio Communications (PIMRC)*, vol. 2. IEEE, 2005, pp. 989–993.

[44] E. Axell, G. Leus, and E. G. Larsson, "Overview of spectrum sensing for cognitive radio," in *2010 2nd International Workshop on Cognitive Information Processing (CIP)*. IEEE, 2010, pp. 322–327.

[45] I. F. Akyildiz, B. F. Lo, and R. Balakrishnan, "Cooperative spectrum sensing in cognitive radio networks: A survey," *Physical communication*, vol. 4, no. 1, pp. 40–62, 2011.

[46] J. Ma, G. Y. Li, and B. H. Juang, "Signal processing in cognitive radio," *Proceedings of the IEEE*, vol. 97, no. 5, pp. 805–823, 2009.

[47] D. Cabric, S. M. Mishra, and R. W. Brodersen, "Implementation issues in spectrum sensing for cognitive radios," in *Conference record of the thirty-eighth Asilomar conference on Signals, systems and computers, 2004.*, vol. 1. IEEE, 2004, pp. 772–776.

[48] A. V. Dandawate and G. B. Giannakis, "Statistical tests for presence of cyclostationarity," *IEEE Transactions on signal processing*, vol. 42, no. 9, pp. 2355–2369, 1994.

[49] O. A. Dobre *et al.*, "Second-order cyclostationarity of mobile WiMAX and LTE OFDM signals and application to spectrum awareness in cognitive radio systems," *IEEE Journal of Selected Topics in Signal Processing*, vol. 6, no. 1, pp. 26–42, 2012.

[50] S. Chaudhari, V. Koivunen, and H. V. Poor, "Autocorrelation-based decentralized sequential detection of OFDM signals in cognitive radios," *IEEE Transactions on Signal Processing*, vol. 57, no. 7, pp. 2690–2700, 2009.

[51] S. Chaudhari, J. Lunden, and V. Koivunen, "Collaborative autocorrelation-based spectrum sensing of OFDM signals in cognitive radios," in *2008 42nd Annual Conference on Information Sciences and Systems*, March 2008, pp. 191–196.

[52] D. Cabric, A. Tkachenko, and R. W. Brodersen, "Spectrum sensing measurements of pilot, energy, and collaborative detection," in *IEEE Military Communications Conference (MILCOM) 2006.* IEEE, 2006, pp. 1–7.

[53] K. W. Martin, "Small side-lobe filter design for multitone data-communication applications," *IEEE Transactions on Circuits and Systems II: Analog and Digital Signal Processing*, vol. 45, no. 8, pp. 1155–1161, 1998.

[54] B. Farhang-Boroujeny and C. H. Yuen, "Cosine modulated and offset QAM filter bank multicarrier techniques: a continuous-time prospect," *EURASIP Journal on Advances in Signal Processing*, vol. 2010, p. 6, 2010.

[55] R. W. Chang, "Synthesis of band-limited orthogonal signals for multichannel data transmission," *Bell Labs Technical Journal*, vol. 45, no. 10, pp. 1775–1796, 1966.

[56] B. Saltzberg, "Performance of an efficient parallel data transmission system," *IEEE Transactions on Communication Technology*, vol. 15, no. 6, pp. 805–811, 1967.

[57] B. Hirosaki, "An orthogonally multiplexed QAM system using the discrete fourier transform," *IEEE Transactions on Communications*, vol. 29, no. 7, pp. 982–989, 1981.

[58] PHYDAS, "FBMC physical layer : a primer," Online, 2010, (Accessed: Apr. 2016). [Online]. Available: http://www.ict-phydyas.org/

[59] A. Viholainen, T. Ihalainen, T. H. Stitz, M. Renfors, and M. Bellanger, "Prototype filter design for filter bank based multicarrier transmission," in *2009 17th European Signal Processing Conference*. IEEE, 2009, pp. 1359–1363.

[60] P. P. Vaidyanathan, *Multirate systems and filter banks*. Pearson Education India, 1993.

[61] P. Siohan, C. Siclet, and N. Lacaille, "Analysis and design of OFDM/OQAM systems based on filterbank theory," *IEEE transactions on signal processing*, vol. 50, no. 5, pp. 1170–1183, 2002.

[62] M. Bellanger *et al.*, "FBMC physical layer: a primer," *PHYDYAS, January*, 2010.

[63] T. Saramaki and Y. Neuvo, "A class of FIR Nyquist (Nth-band) filters with zero intersymbol interference," *IEEE transactions on circuits and systems*, vol. 34, no. 10, pp. 1182–1190, 1987.

[64] M. G. Bellanger, "Specification and design of a prototype filter for filter bank based multicarrier transmission," in *IEEE International Conference on Acoustics, Speech, and Signal Processing, 2001, (ICASSP'01).*, vol. 4. IEEE, 2001, pp. 2417–2420.

[65] M. Aldababseh, "Channel estimation for FBMC/OQAM wireless system based on Kalman filter," Master's thesis, Al-Quds University, 2010.

[66] U. Madhow, *Introduction to Communication Systems*. Cambridge, 2014.

[67] P. Stoica and R. L. Moses, *Introduction to spectral analysis*. Prentice hall Upper Saddle River, 1997, vol. 1.